

Numerical Simulations of Island-Scale Airflow over Maui and the Maui Vortex under Summer Trade Wind Conditions

DANA L. CARLIS*

*Howard University Program in Atmospheric Sciences, Washington, D.C., and Honolulu Weather Forecast Office,
National Weather Service, Honolulu, Hawaii*

YI-LENG CHEN

Department of Meteorology, University of Hawaii at Manoa, Honolulu, Hawaii

VERNON R. MORRIS

Howard University Program in Atmospheric Sciences, Howard University, Washington, D.C.

(Manuscript received 22 September 2009, in final form 14 January 2010)

ABSTRACT

The fifth-generation Pennsylvania State University–NCAR Mesoscale Model (MM5) coupled with the Noah land surface model (LSM) is employed to simulate island-scale airflow and circulations over Maui County, Hawaii, under summer trade wind conditions, during July–August 2005. The model forecasts are validated by surface observations with good agreement.

In this study, it is shown that a previously known closed circulation over the Central Valley of Maui, or the Maui vortex, represents the northern cyclonic vortex of the dual-counter-rotating vortices in the lee of Haleakala, which extend up to the base of the trade wind inversion with a westerly reversed flow ($>2 \text{ m s}^{-1}$). At low levels, the northern cyclonic vortex is more pronounced than the southern anticyclonic vortex. The asymmetric structure of the dual vortices is related to the shape of Haleakala and the flow deflection by the West Maui Mountains. The Maui vortex has a relatively narrow east–west extent in the lowest levels, especially at night, due to the deflected strong northerly/northeasterly winds from the windward foothills of the West Maui Mountains. Unlike the lee vortices off the leeward coast of the island of Hawaii, the Maui vortex and the westerly return flow in low levels are mainly over land and are strongly modulated by the diurnal heating cycle. In addition, the location and horizontal and vertical extent are affected by the trade wind speed and latent heat release.

Over the West Maui Mountains, with their height below the trade wind inversion, dual-counter-rotating vortices are present below the 1-km level in the wake, with strong downslope flow on the leeward slopes followed by a hydraulic jump. In the afternoon, downslope winds are weak, with combined westerly return/sea-breeze flow along the leeward coast. Orographic blocking is also evident over eastern Molokai with strong downslope winds, especially at night.

1. Introduction

Most of the previous studies of island-induced airflow and weather over the Hawaiian Islands have focused on

the largest island of the Hawaiian Island chain, the island of Hawaii (also known as the “Big Island”), with several international field programs. The latest field campaign, the Hawaiian Rain Band Project (HaRP), was conducted in July–August 1990 (Chen and Nash 1994). Even though considerable advances in the understanding of island effects under trade wind weather have been made from numerous studies over the island of Hawaii (Lavoie 1967; Garrett 1980; Nickerson and Dias 1981; Smolarkiewicz et al. 1988; Smith and Grubišić 1993; Carbone et al. 1995; Austin et al. 1996; Esteban and Chen 2008; and others), studies of island circulations and

* Current affiliation: National Centers for Environmental Prediction/Environmental Modeling Center, Camp Springs, Maryland.

Corresponding author address: DaNa L. Carlis, NCEP/EMC, 5200 Auth Rd., Room 207, Camp Springs, MD 20746.
E-mail: dana.carlis@noaa.gov

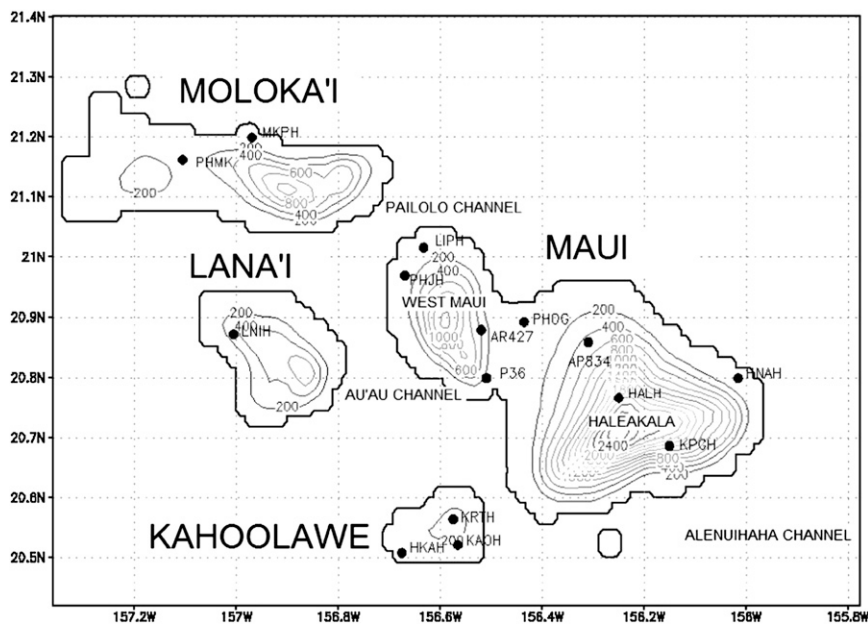


FIG. 1. Map of Maui County showing station locations and terrain (every 200 m).

local weather over the island of Maui are few (Daniels and Schroeder 1978; Ueyoshi et al. 1996). The topography of Maui is dominated by two mountains, Haleakala (height ~ 3055 m) to the east and the West Maui Mountains (height ~ 1764 m) (Fig. 1). The mountains are connected by a flat isthmus (i.e., the Central Maui Valley). The Maui vortex is one of the dominant circulation features over the Central Valley of Maui. The vortex circulation is most significant at the 1-km level, with a return to trade wind flow at the 2-km level (Leopold 1949). The importance of the Maui vortex is its ability to trap pollutants due to agricultural burning, which makes it an important feature for the forecasters at the Honolulu Forecast Office (Schroeder 1993).

Most of the previous theoretical studies on airflow past 3D mountains are based on idealized studies (e.g., Smolarkiewicz et al. 1988; Smolarkiewicz and Rotunno 1989; Schär and Smith 1993; Rotunno et al. 1999; Schär and Durran 1997; Epifanio and Rotunno 2005). For $U/N > h$ (where N is the Brunt–Väisälä frequency, U is the cross-mountain wind speed, and h is the mountain height), the surface air parcels flow almost directly over the mountain, with a large-amplitude gravity wave over the peak (Smolarkiewicz et al. 1988). Under normal trade wind conditions with $U \sim 7$ m s $^{-1}$, Nguyen et al. (2010) showed that U/N averaged over the 300–600-m layer is about 1500 m. With terrain height ~ 900 m, the flow regime past the Ko‘olua Mountains over Oahu is dominated by the “flow over” regime, with mountain waves above the peak. Nguyen et al. (2010) showed that the westerly reversed flow off the western leeside coast of

Oahu in the afternoon is mainly thermally driven and is limited to the lowest levels near the surface (< 1 km). For U/N much smaller than h , the low-level flow is diverted around the flanks of the mountain. Smolarkiewicz and Rotunno (1989) simulated lee vortex formation in stratified flow past a three-dimensional obstacle under a low (< 1) Froude number ($Fr = U/Nh$) flow regime. They attribute lee vortex formation past a 3D obstacle flow to be a purely inviscid process. Leopold (1949) showed that for mountains with tops well above the trade wind inversion (~ 2 km in Hawaii), the inversion serves as a lid forcing the low-level flow to be deflected by the terrain (Schär and Smith 1993). Chen and Feng (2001) showed that for the island of Hawaii, with peaks well above the trade wind inversion, in addition to Fr , the island-scale airflow and weather are affected by the trade wind inversion height.

Reisner and Smolarkiewicz (1994) studied low (< 1) Fr flow past a 3D obstacle with uniform heating at the surface and obtained a simple criterion for the transition from blocked flow to unblocked flow. Diabatic heating could also affect flow transition, namely, flow over and flow around a mesoscale mountain (Miglietta and Buzzi 2001; Colle 2004). Studies over the island of Hawaii reveal that the island-scale airflow and weather are modulated by the diurnal heating cycle (Chen and Nash 1994; Feng and Chen 1998; Yang and Chen 2003). The feedback effects associated with clouds and precipitation strengthen orographic lifting while reducing perturbation surface pressure on the windward side, resulting in weaker orographic blocking (Chen and Feng 2001).

Previous observational (Chen and Wang 1995; Carbone et al. 1995; Li and Chen 1999; Frye and Chen 2001) and modeling (Feng and Chen 2001) studies show that rain evaporative cooling affects the onset, depth, strength, and offshore extent of the katabatic flow.

Zhang et al. (2005a, hereafter Z05a) showed that with increased model resolution and improved land surface parameters, surface meteorological variables for the main airport sites over Oahu were well simulated throughout the diurnal cycle using the regional spectral model (Juang 2000) coupled with the Oregon State University, Air Force, and National Weather Service (NWS) Office of Hydrology (Noah) land surface model (LSM). Using the fifth-generation Pennsylvania State University–National Center for Atmospheric Research (PSU–NCAR) Mesoscale Model (MM5; Dudhia 1993), Yang et al. (2005) showed that without using the LSM, the simulated ground temperature in the afternoon at the semi-arid regions of Mauna Kea and Mauna Loa on the island of Hawaii during HaRP is more than 20°C lower than observed (32° versus 12°C; see their TEST1). With improved land surface parameters (Z05a), together with the LSM, their simulated ground temperature is in good agreement with observations. In their study, from 50 Portable Automatic Mesonet (PAM) surface datasets alone, there are approximately 50 000 ($50 \times 24 \times 45$) hourly data pairs, from the 45 days during HaRP, for simulation versus observation comparisons. Yang et al. (2005) and Yang and Chen (2008) successfully simulated the diurnally driven circulation cells on both the windward and lee sides of the island of Hawaii. For the island of Maui, there are large variations in landscape, ranging from tropical rain forest on the windward side to semi-arid regions on the lee side of mountains and above the trade wind inversion. Thus, careful treatment of land surface forcing in the model is important.

For the wake circulations of the island of Hawaii, the dual-rotating lee vortices occur off the leeside coast and extend several hundred kilometers downstream over the ocean (Smith and Grubišić 1993). Regarding the Maui vortex, it occurs mainly over the Central Valley, with a single closed cyclonic circulation and a relatively small (~20 km) horizontal extent (Leopold 1949). It is postulated that the low-level trade wind flow is channeled through the Central Valley between the West Maui Mountains and Haleakala volcano; the flow is then diverted eastward by a combination of flow deflection by the West Maui Mountains and the daytime anabatic/upslope winds on the leeside slopes of Haleakala, with a closed vortex circulation over the Central Valley (Ueyoshi et al. 1996; Kodama and Businger 1998). The vortex circulation is more pronounced under stronger trade winds. Numerical simulations by Ueyoshi et al.

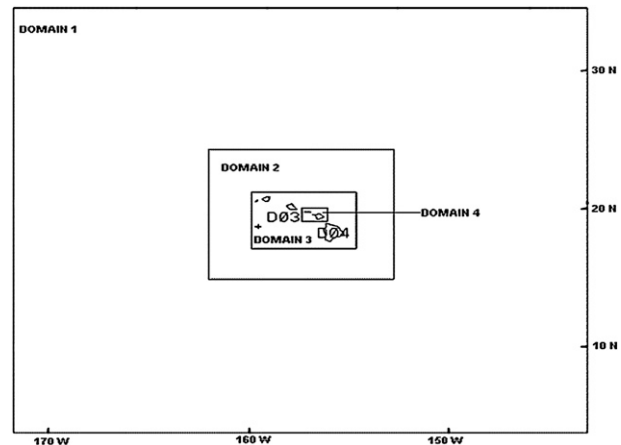


FIG. 2. Two-way nested domains from the MM5/LSM simulations. The grid spacing for domains 1–4 is 54, 18, 6, and 2 km, respectively.

(1996, hereafter U96) suggest that the Maui vortex may exist at night with a much weaker circulation.

In this work, we would like to address factors that account for the existence, horizontal extent, and location of the Maui vortex, as well as the impact of thermal forcing from the surface on its diurnal evolution. Is the Maui vortex a result of orographic blocking by Haleakala? Is it affected by the orographic blocking of the West Maui Mountains? Is the daytime heating over land essential for its existence? How does the diurnal heating cycle affect its structure, horizontal extent and location? How does the trade wind strength affect its intensity, location, and horizontal extent? Toward this end, we will use the MM5/LSM model with improved land surface conditions to study the structure of the Maui vortex over the Central Valley. The surface data collected over our model domain will be used to validate our model results.

2. MM5/LSM model description and initialization

In this study, the MM5 model (version 3.6.3) coupled with the LSM (Chen and Dudhia 2001a,b), with four nested domains at horizontal resolutions of 54, 18, 6, and 2 km (Fig. 2), is used with two-way nesting procedures. The model's initial conditions are obtained from the daily Global Forecast System (GFS). The resolution of the GFS is $1^\circ \times 1^\circ$. We employ a high-resolution global SST analysis from the National Centers for Environmental Prediction (NCEP) that has a $0.5^\circ \times 0.5^\circ$ resolution. The soil temperature and soil moisture parameters provided by the GFS model are not used in the initial conditions because most GFS grid points over the Hawaiian Islands are ocean points. We employed 36 sigma levels from

TABLE 1. Locations and names of stations used in this study with station elevations and available data types for each station. The surface variables are wind speed (WS), wind direction (WD), temperature (T), dewpoint temperature (TD), and relative humidity (RH; %). Boldface indicates MADIS archive data.

Name	Station ID	Lat	Lon	Elev (m)	Model elev (m)	Island	Surface variables
Kahului Airport	PHOG	20.9	-156.4	15.9	8.0	Maui	T , TD, WD, WS
Hana AP	HNAH	20.8	-156.0	185.9	14.7	Maui	WD, WS
Kaupo Gap	KPGH	20.7	-156.2	1222.2	1422.5	Maui	T , WD, WS, RH
Kapalua West Maui	PHJH	21.0	-156.7	39.9	59.0	Maui	T , TD, WD, WS
Ma'alaea Bay	P36	20.8	-156.5	3.1	101.6	Maui	WD, WS
Lipoa	LIPH	21.0	-156.6	45.7	28.9	Maui	WD, WS
Haleakala	HALH	20.7	-156.3	2121.4	1748.1	Maui	WS, WD
AP834	APMI	20.9	-156.5	264.6	234.8	Maui	T, TD, WS, WD
AR427	ARMI	20.9	-156.3	497.1	470.5	Maui	T, TD, WS, WD
Makapulapai	MKPH	21.2	-157.0	22.9	87.1	Molokai	T , WD, WS, RH
Molokai Airport	PHMK	21.2	-157.1	137.2	132.5	Molokai	T , TD, WD, WS
Lanai 1	LNHI	20.9	-157.0	387.1	284.5	Lanai	T , WD, WS, RH
Kahoolawe ARC	KRTH	20.6	-156.6	365.8	329.1	Kahoolawe	T , WD, WS
Kaneloa	KAOH	20.5	-156.6	248.4	114.9	Kahoolawe	T , WD, WS
Honokanai'a	HKAH	20.5	-156.7	21.3	7.8	Kahoolawe	T , WD, WS

the surface to the 100-hPa level, with 13 levels below $\sigma = 0.9$.¹ The Grell (1993) cumulus parameterization was used along with the shallow grid-scale warm rain process (Chen and Avissar 1994a,b; Hsie et al. 1984), a cloud-radiation scheme (Dudhia 1989), and Hong and Pan's (1996) Medium-Range Forecast boundary layer scheme.

Over Maui, the MM5 model has two vegetation types (i.e., mixed forest and urban) and three soil types (i.e., silt loam, clay, and clay loam). In this study, we use the 30-s resolution (~ 1 km) vegetation type, and the soil type and vegetation fraction compiled by Z05a. Similar to Z05a, prior to the study period (1 July–31 August 2005), the MM5/LSM model was run once per day initialized at 0000 UTC for a 2-month period using the previous day's 24-h forecasts of soil parameters. During the period of study, the model runs were 36-h forecasts, with the results from hours 12 through 35 used to represent the diurnal cycle for each day. In addition, we examine the role of island blocking by comparing differing trade wind flow regimes (strong versus weak) over Maui. The strong and weak trade wind regimes are characterized by the daily GFS 0000 UTC forecast wind data at the 1000-hPa level for an upstream point (21°N, 155°W). The six strong ($U \geq 8 \text{ m s}^{-1}$) trade wind days are 7, 8, 17, and 28 July and 1 and 2 August. The six weak ($U \leq 6 \text{ m s}^{-1}$) trade wind days are 10 and 30 July and 12, 18, 25, and 27 August.

¹ The sigma levels used by the MM5/LSM model are the following: 1.0, 0.999, 0.998, 0.996, 0.994, 0.992, 0.990, 0.988, 0.985, 0.980, 0.970, 0.945, 0.91, 0.90, 0.865, 0.820, 0.790, 0.760, 0.730, 0.700, 0.670, 0.640, 0.610, 0.580, 0.550, 0.520, 0.475, 0.425, 0.375, 0.325, 0.275, 0.225, 0.175, 0.125, 0.075, and 0.025.

To test the impacts of the West Maui Mountains, land surface forcing, and latent heat release on the development and structure of the Maui vortex, model sensitivity tests are performed for a typical trade wind day on 6 August. The trade wind inversion height on 6 August is at 1.8 km, with the upstream trade wind speeds about 7 m s^{-1} .

3. Validation of the MM5/LSM results over Maui County

Using the land surface characteristics compiled by Z05a, the MM5/LSM model is validated against hourly surface data collected during 1 July–31 August 2005 across Maui County (station locations shown in Fig. 1). Data for two of these stations are from the archive of the Meteorological Assimilation Data Ingest System (MADIS). The rest of the surface data are from the archive of the NWS Honolulu Forecast Office. The grid-point values from the model output were interpolated to station locations using a weight-distance average to the four grid points nearest the station location (Nguyen et al. 2010). Because of the presence of steep terrain, even with a 2-km grid, there were still some differences between actual station elevation and model terrain (Table 1). The simulated 2-m temperature at each station was adjusted to the actual terrain height using the typical temperature lapse rate in the environment.

a. July and August 2005 synoptic conditions

The synoptic weather patterns over the central and North Pacific for July 2005 were dominated by an elongated subtropical high pressure cell to the north of the Hawaiian

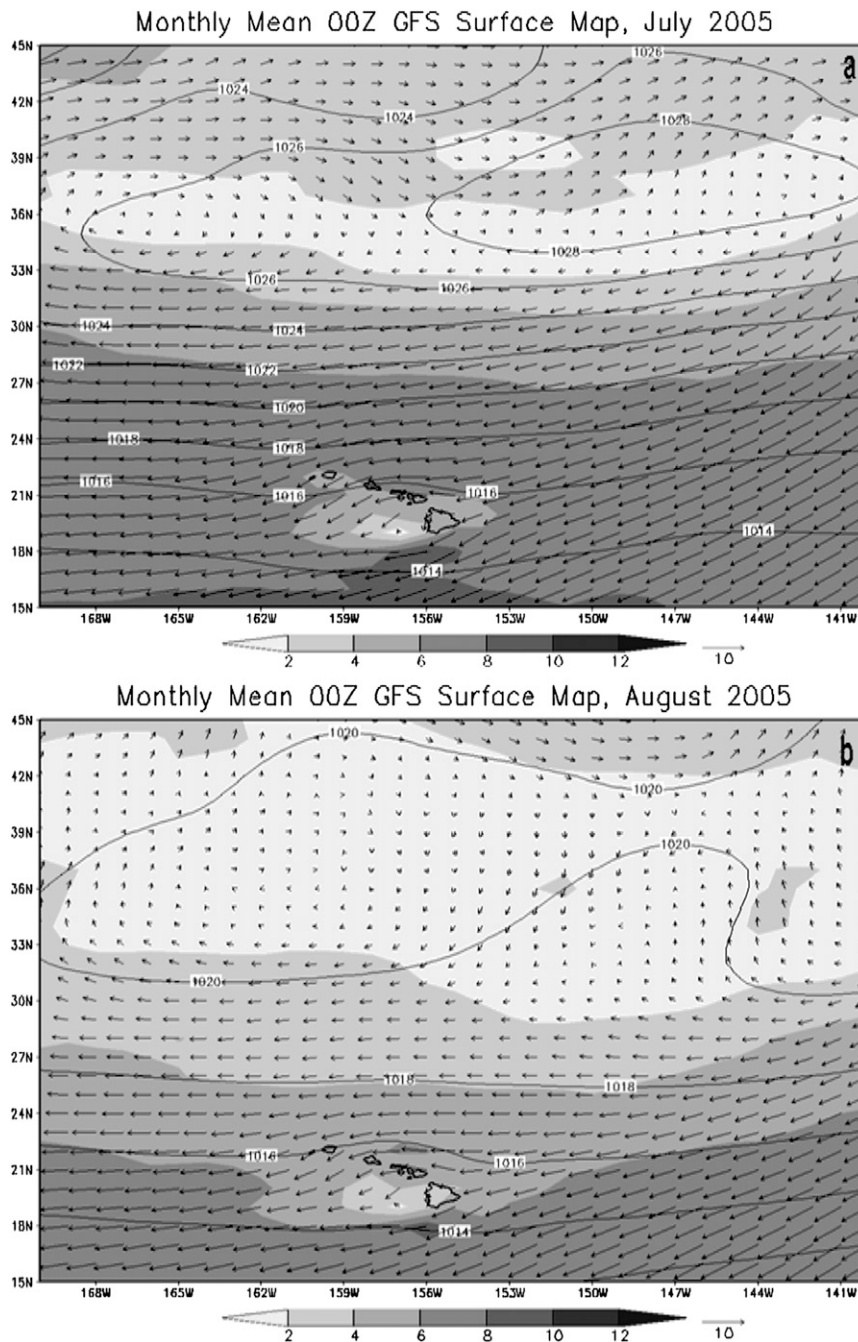


FIG. 3. Mean sea level pressure (isobars every 2 hPa) over the northeast Pacific using the Global Forecast System (GFS) initial conditions during the months of (a) July and (b) August 2005.

Islands, with maximum pressure ~ 1028 hPa (Fig. 3a). Under normal summer trade wind weather, the flow is characterized by easterly trades $\sim 6\text{--}8$ m s^{-1} on more than 93% of occurrences (Schroeder 1993). During August 2005 (Fig. 3b), the high pressure cell split into two separate cells and shifted to the east, forming an elongated cell

closer to California than during the month of July. The mean open ocean trade wind speed for August was slightly weaker than July (~ 6 versus 7 m s^{-1}) but was still within the typical trade wind speed range. Thus, the simulated averaged diurnal cycle for these two months is representative of normal summer trade wind conditions.

TABLE 2. Mean simulated and observed 10-m u - and v -wind speeds, 2-m temperature, and 2-m dewpoint temperature from all stations with available data over Maui County.

All times	10-m u -wind component (m s^{-1})	10-m v -wind component (m s^{-1})	2-m temperature ($^{\circ}\text{C}$)	2-m dewpoint ($^{\circ}\text{C}$)
Mean simulation	-4.3	-1.7	24.3	17.8
Mean obs	-4.8	-2.4	24.6	18.3
Bias	0.5	0.7	-0.3	-0.5
MAE	2.2	2.0	1.7	2.1
RMSE	3.0	2.7	2.4	3.2

b. 62-day error statistics

Error statistics are calculated including bias (simulation - observation), mean absolute error (MAE) or forecast error, and root-mean-square error (RMSE) for 10-m winds and 2-m temperatures and dewpoints (Table 2) using all the available data for each station from the archive. From the error statistics, the forecasts of 2-m temperature and 2-m dewpoint temperature are in reasonable agreement with surface observations. The Makapulapai (MKPH) station (elevation 22.9 m), situated on the northern coast of Molokai, exhibits the largest differences between the observed and simulated surface temperatures (3°C).

Horizontal distributions of mean observed and simulated winds for Maui County are shown in Fig. 4. The simulated winds (Table 2) agree with observations reasonably well. There are two stations within the Central Valley, Kahului International Airport (PHOG) along the northern part of the valley, and Ma'alaea Bay (P36) on the southwestern coast of Haleakala. The wind direction for both the observed and simulated data shows good agreement at both stations. The largest error exists at Kaupo Gap (KPGH) on the southeastern slopes of Haleakala (Fig. 4).

The model predictions exhibit a slight warm (cold) bias at night (day) for 2-m temperatures (Tables 3 and 4). Simulated winds at 0500 and 1400 Hawaii standard time (HST) are consistent with the observed wind data (Fig. 4), with the largest difference at KPGH on the southeastern slopes of Haleakala as the daytime upslope flow there is not well simulated (Fig. 4c).

4. Mean island-scale airflow over Maui County

a. Mean surface airflow

Hourly model results are averaged for the entire 62-day period to produce the mean state fields. The incoming trade wind flow decelerates significantly on the windward side and is deflected around the topography, with weak southeasterlies (1.5 m s^{-1}) over the northeastern coast and northeasterlies (4.5 m s^{-1}) off the southeastern coast (Fig. 5a). Upstream of the West Maui Mountains flow deceleration is also prevalent. On the lower

windward slopes of eastern Molokai a weak wind region ($<4 \text{ m s}^{-1}$), due to flow deceleration, is also simulated.

The Maui vortex, in the lee of Haleakala, is successfully simulated at the surface, with strong ($\sim 8\text{--}9 \text{ m s}^{-1}$) easterly winds over the northern part of the valley downstream of the northern ridge axis of Haleakala, strong ($\sim 8\text{--}9 \text{ m s}^{-1}$) northwesterly winds along the eastern foothills of the West Maui Mountains and off the leeside coast of Haleakala, and weak ($\sim 2 \text{ m s}^{-1}$) southerly flow along the lower leeside slopes of Haleakala parallel to the terrain (Fig. 5a). The horizontal extent ($\sim 10 \text{ km}$) of the vortex is in agreement with previous observations (Leopold 1949). The strong winds, with cyclonic curvature downstream of the northern ridge axis of Haleakala, impinge on the West Maui Mountains resulting in flow splitting on the windward side, with strong northeasterly winds along the windward foothills of the West Maui Mountains. The strongest surface winds ($>8 \text{ m s}^{-1}$) over Maui County are simulated on the southeastern leeside slopes of the West Maui Mountains and the adjacent coast. This area, Ma'alaea Bay, is one of the windiest spots in Hawaii. Strong downslope winds are also simulated on the northwestern leeside slopes of West Maui and eastern Molokai (Fig. 5a). Over the southern leeside of Haleakala, the flow exhibits anticyclonic shear, between weak winds in the lee and strong easterly winds moving around the southern coast of Haleakala.

Strong gap winds are simulated within the Alenuihaha Channel (Zhang et al. 2005b) between East Maui and the northwest portion of the island of Hawaii, with an average wind speed of 10 m s^{-1} (Fig. 5a). The island of Kahoolawe is downstream of the Alenuihaha Channel, with relatively strong winds (Fig. 5a). Within the Pailolo Channel, between Molokai and West Maui, there is also an increase in wind speeds ($\sim 9 \text{ m s}^{-1}$). Northern Lanai is downstream of the Pailolo Channel with relatively strong winds. Strong winds ($>8 \text{ m s}^{-1}$) are also simulated within the ocean channel between Molokai and Oahu and offshore of the northern corner of Haleakala.

b. Mean horizontal airflow above the surface

In contrast to previous observations and simulations (Leopold 1949; U96) that show only a single vortex over

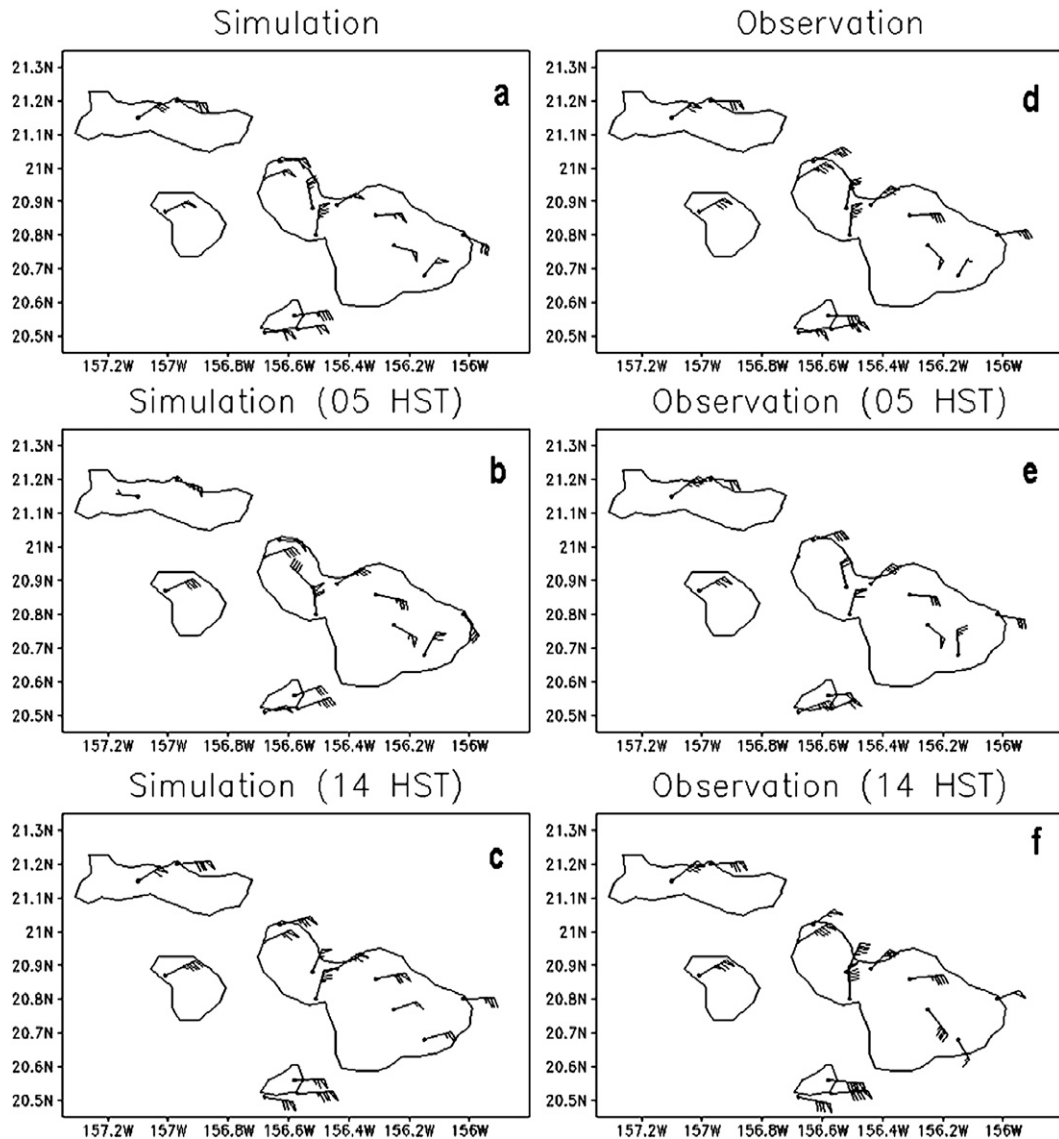


FIG. 4. The 62-day (1 July–31 August) 10-m winds: (a) simulated 24-h mean winds, (b) simulated at 0500 HST, (c) simulated at 1400 HST, (d) observed 24-h mean winds, (e) observed at 0500 HST, and (f) observed at 1400 HST. Winds in m s^{-1} with pennant, full barb, and half barb representing 5, 1, and 0.5 m s^{-1} , respectively. Wind barb convention is the same hereafter.

the Central Valley, our model results indicate that, at the 0.5-km level, the lee sides of both Haleakala and the West Maui Mountains are dominated by dual-counter-rotating vortices with a westerly return flow in between

(Fig. 5b). The dual vortex structure consists of a pronounced cyclonic circulation to the north and a relatively weak anticyclonic circulation to the south. Similar to the large wake off the island of Hawaii, the simulated

TABLE 3. As in Table 2, but for the 0500 HST mean.

0500 HST	10-m u -wind component (m s^{-1})	10-m v -wind component (m s^{-1})	2-m temperature ($^{\circ}\text{C}$)	2-m dewpoint ($^{\circ}\text{C}$)
Mean simulation	-2.8	-1.4	22.7	17.1
Mean obs	-3.8	-2.1	22.2	17.2
Bias	1.0	0.7	0.5	-0.1
MAE	2.3	1.9	1.5	1.9
RMSE	3.0	2.4	1.9	2.3

TABLE 4. As in Table 2, but for the 1400 HST mean.

1400 HST	10-m u -wind speed (m s^{-1})	10-m v -wind speed (m s^{-1})	2-m temperature ($^{\circ}\text{C}$)	2-m dewpoint ($^{\circ}\text{C}$)
Mean simulation	-5.4	-1.8	26.5	17.9
Mean obs	-5.7	-2.7	27.9	18.7
Bias	0.4	0.9	-1.4	-0.8
MAE	2.1	2.0	2.1	2.2
RMSE	2.7	2.7	2.6	3.6

flow regime over Haleakala is characterized by the inability of the flow to move over the mountain, as the trade wind inversion height serves as a lid (Leopold 1949; Schär and Smith 1993).

For the lowest levels, especially at the surface, the lee vortices are significantly affected by the orographic blocking of the West Maui Mountains (MM5/LSM max height ~ 1250 m), with a relatively narrow east–west extent

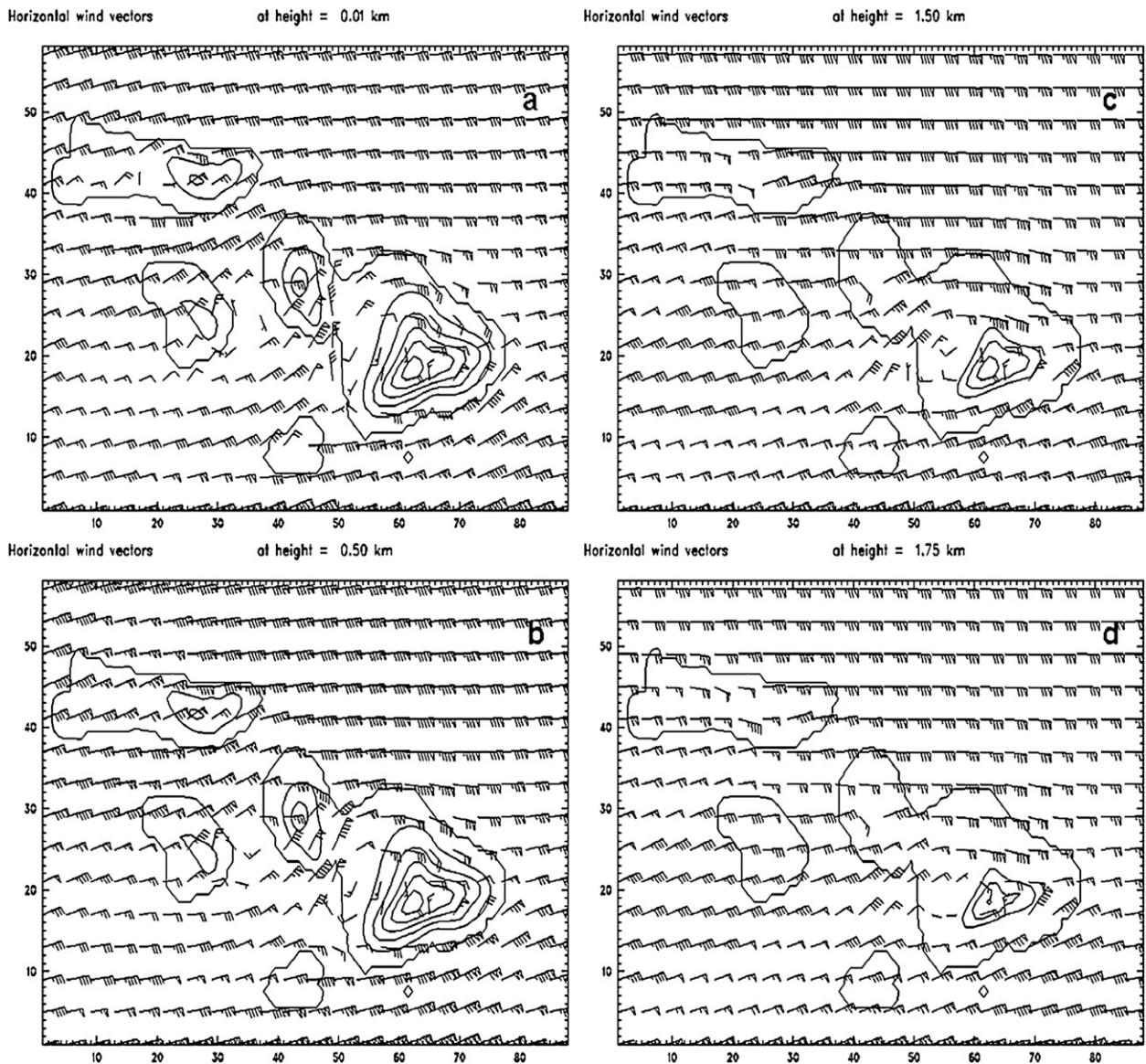


FIG. 5. Simulated 62-day mean horizontal winds at (a) the surface, (b) the 0.5-km level, (c) the 1.5-km level, and (d) the 1.75-km level. Terrain contours every 500 m showing the terrain above each height level.

because of the strong orographically induced northerly/northeasterly winds off the western leeside coast of Haleakala (Fig. 5a). At the 1.5-km level, with less influence from orographic blocking by the West Maui Mountains as compared with the surface, and with Haleakala having a more circular shape at higher elevation, the southern anticyclonic vortex is clearly evident (Fig. 5c). Furthermore, the Maui vortex extends farther off the western leeside coast of Haleakala aloft compared to the surface.

U96 shows a discernible vortex up to an altitude of about 1100 m MSL. Leopold (1949) estimated the vortex to exist up to 1200 m MSL. Our simulated horizontal winds at the 1.5- and 1.75-km levels (Figs. 5c,d) show the dual vortices along the lee slopes of Haleakala, with the horizontal extent decreasing with height. From aircraft flight-level data, Smith and Grubišić (1993) showed that the wake in the lee of the island of Hawaii consists of two counter-rotating eddies that exist up to a height of 1700 m, which is more aligned with our results.

5. Impact of the West Maui Mountains on the Maui vortex

U96 stated that “two major factors, solar heating and accelerated northerly flow over the valley resulting from deflection of trades by West Maui, appear to contribute to the formation and maintenance of the Maui vortex.” To investigate the impact of the West Maui Mountains on the Maui vortex, we conduct a model sensitivity test by removing the West Maui Mountains in the model (NWM) for a typical trade wind day, 6 August 2005. The NWM run is initialized at 1400 HST 5 August and run for a 36-h simulation. The model data between hours 12 and 35 (0200 HST 6 August–0100 HST 7 August) represents the full diurnal cycle.

At the surface, the NWM run shows east–west-elongated dual-counter-rotating vortices over the Central Valley that extend more than 20 km downstream from the foothills of Haleakala (Fig. 6a). Because of the geometry of Haleakala, the dual-rotating vortices simulated by the NWM run are not symmetric. The impinging angle of the incoming trade wind flow with the terrain is relatively large for the convex-shaped northern ridge axis of Haleakala, whereas along the southern coast, the terrain contours are parallel to the incoming flow. As a result, the northern cyclonic vortex dominates most of the Central Valley, with a weaker anticyclonic vortex to the south. At the 1-km level, the dual-counter-rotating vortices become more symmetric in the NWM run (Fig. 6b), as the shape of Haleakala becomes more circular at a higher elevation.

In the control run, with full model physics and model terrain (CTRL), the Maui vortex at the surface has a limited east–west extent, with strong northerly/northeasterly winds

dominating the western leeside coast of Haleakala as a result of orographic blocking by the West Maui Mountains (Fig. 6c). For the CTRL, the northern cyclonic vortex is elongated in the north–south direction as compared with the NWM run where the center of the vortex has shifted southwest with westerly return flow over the channel. The southern anticyclonic vortex at the surface is not discernable. At the 1-km level, with less significant orographic blocking by the West Maui Mountains than at the surface, dual-counter-rotating vortices are evident in the lee of Haleakala for the CTRL run (Fig. 6d) but are less symmetric, with a smaller east–west extent as compared to the NWM run.

The westerly return flow and the counter-rotating vortices in the lee of Haleakala extend to approximately the 1.8-km height level in the NWM run (Figs. 7a,b). In the CTRL run, with orographic blocking by the West Maui Mountains, the westerly return flow in low levels is less significant (Fig. 7c) than NWM (Fig. 7a). However, with strong northerly flow from the foothills of the West Maui Mountains in the CTRL (Fig. 6c), the low-level cyclonic vorticity associated with the Maui vortex is larger in the CTRL (Fig. 7d) as compared to NWM (Fig. 7b).

The above results attest that the Maui vortex is mainly a result of orographic blocking by Haleakala. The Maui vortex represents the northern cyclonic lee vortex, which is more pronounced than the southern anticyclonic lee vortex. The asymmetric dual-vortex structure is caused by orographic blocking by the West Maui Mountains and the noncircular shape of Haleakala. The southern anticyclonic vortex may also be affected by the island of Kahoolawe off the southwestern leeside coast. In contrast to the lee vortices for the island of Hawaii, the Maui vortex is mainly over land. The impact of land surface forcing on the Maui vortex during the diurnal cycle will be presented in the following sections.

6. Airflow at 0500 HST

a. Horizontal view

At the surface, the upwind flow deceleration and flow splitting along the windward side of Haleakala at 0500 HST are more significant (Fig. 8a) than the mean flow (Fig. 5a), with weak ($<2 \text{ m s}^{-1}$) westerly katabatic winds on the eastern end of Haleakala. Over the northeastern and southeastern slopes of Haleakala, the surface flow exhibits an offshore/downslope wind component. Over West Maui, orographic blocking of the strong winds downstream of the convex northern coastline of Haleakala by the West Maui Mountains is significant. Flow splitting is simulated over the windward foothills, with strong ($\sim 8 \text{ m s}^{-1}$) northerly winds downstream off the western leeside coast of Haleakala (Fig. 8a). Over the windward

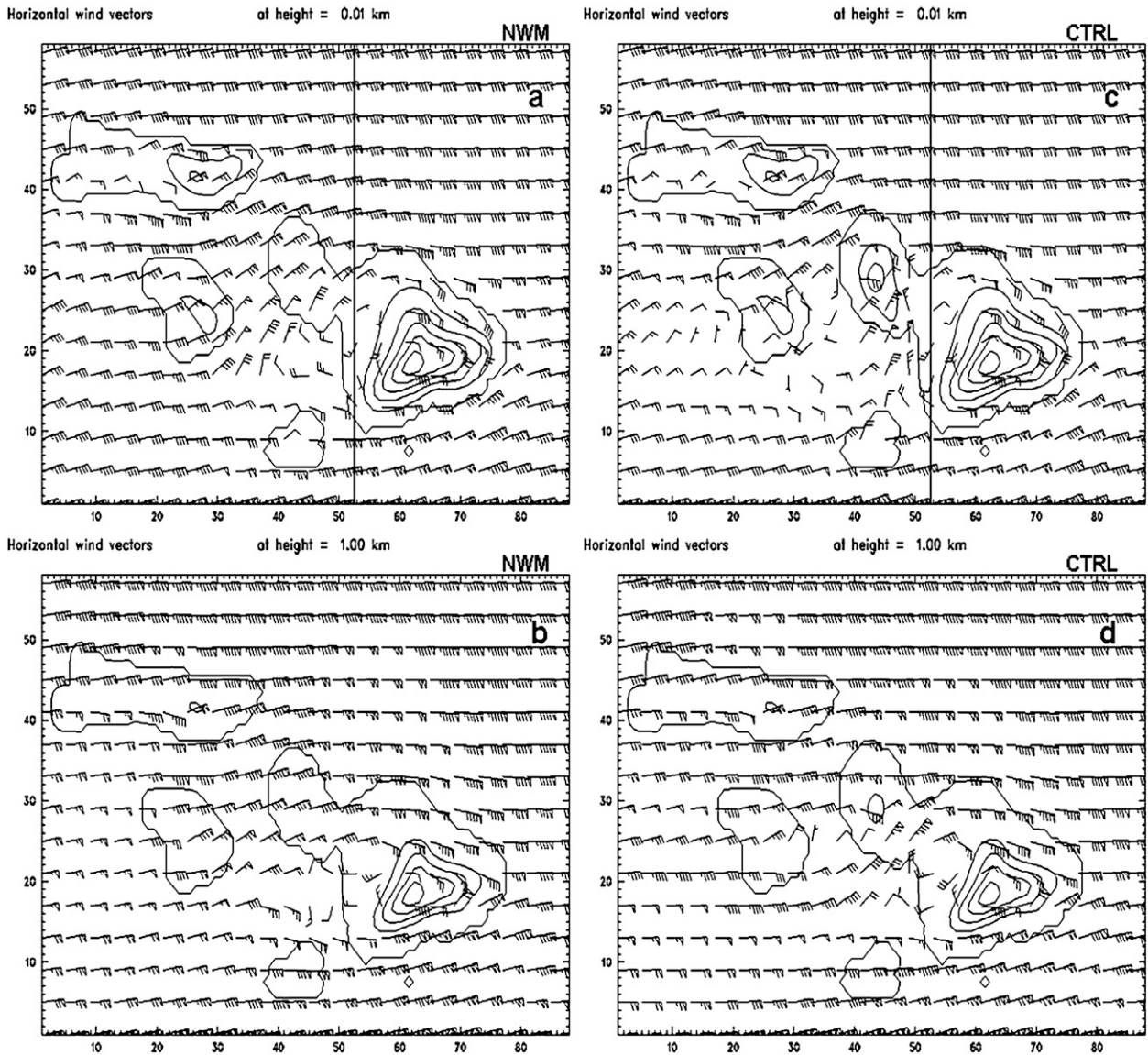


FIG. 6. Simulated 24-h mean winds for the 6 Aug 2005 case: (a) NWM run at the 10-m level, (b) NWM run at the 1-km level, (c) CTRL run at the 10-m level, and (d) CTRL run at the 1-km level. Solid lines in (a) and (c) represent the north–south vertical cross section along the axis of the dual-counter-rotating vortices. Terrain contours every 500 m showing the terrain above each height level.

foothills of the West Maui Mountains, winds exhibit a downslope wind component as a combination of orographic blocking and nighttime cooling. Over the Au’au Channel, off the leeside coast of the West Maui Mountains, wake circulations exist with a weak return flow offshore ($\leq 2 \text{ m s}^{-1}$).

Over the western leeside slopes of Haleakala, the surface flow at night is characterized by weak katabatic flow (Fig. 8a). A weak cyclonic vortex is simulated over the Central Valley at the surface, with a smaller horizontal extent compared to the mean state. The difference between the surface air temperature and upstream

air temperature, at the same height, at 0500 HST (Fig. 8c) is about -1 to -2 K , with the smallest anomalies ($< -1 \text{ K}$) along the lee sides of mountains (e.g., the southeastern and western lee sides of Haleakala, the leeside of the Western Maui Mountains, the southern leeside of Molokai), as well as over the relatively small islands with low terrain (i.e., Lanai and Kahoolawe).

At the 1.5-km level, the dual-rotating vortices and the westerly return flow are well defined over the Central Valley (Fig. 8b). It is apparent that daytime heating is not essential for the existence and maintenance of the Maui vortex. With the presence of easterly katabatic

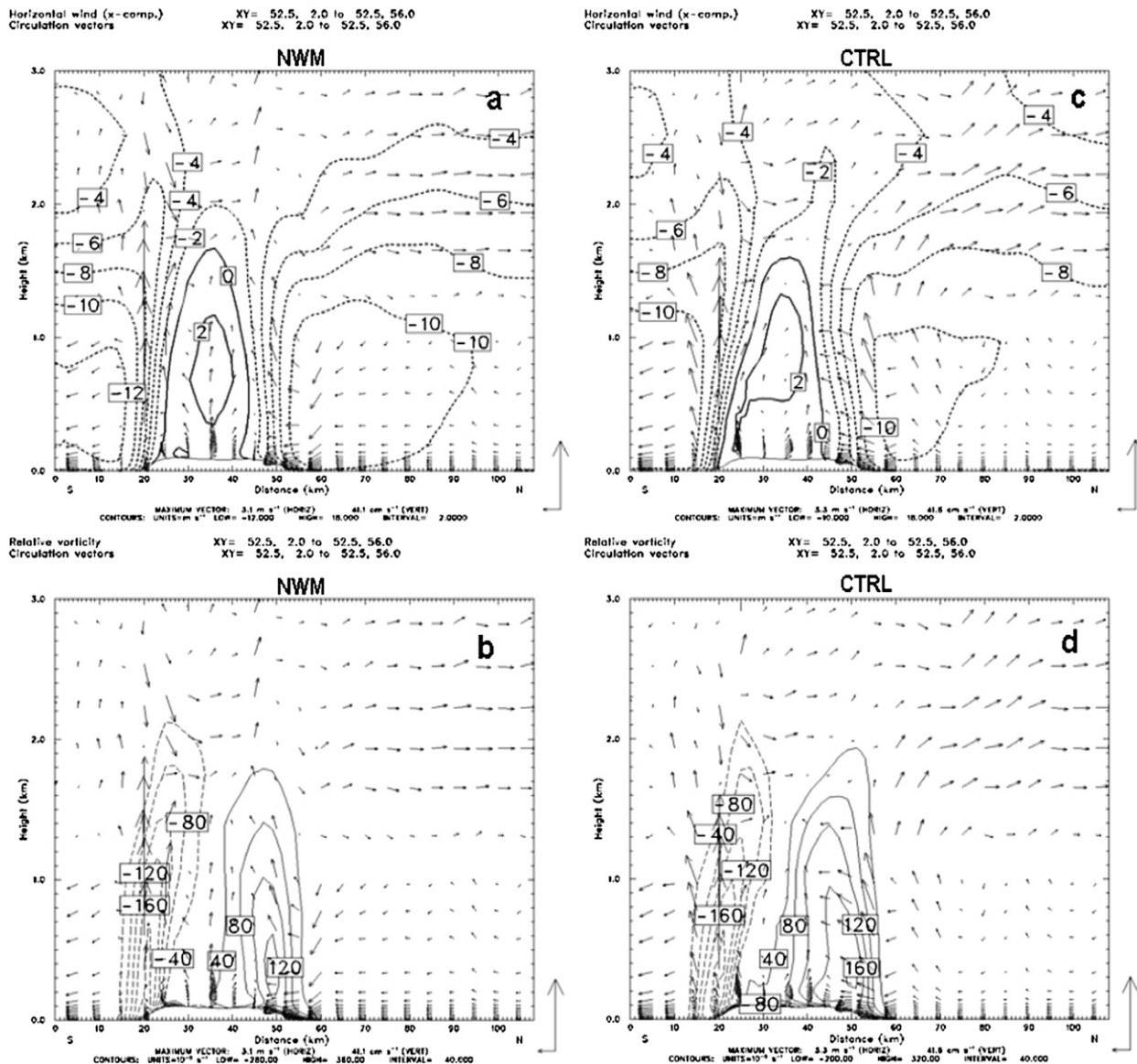


FIG. 7. North-south vertical cross section (Fig. 6a): (a) u -wind component from the NWM run (every $2 m s^{-1}$) and (b) relative vorticity from the NWM run (every $40 \times 10^{-5} s^{-1}$). (c),(d) As in (a),(b), but for the CTRL run.

flow in low levels, the westerly return flow at the 1.5-km level is slightly enhanced, with a slightly larger horizontal extent than the mean state (Fig. 5c). Further discussion of diurnally induced flow on the leeside slopes of Haleakala will be presented in section 8.

b. Vertical structure of the Maui vortex at 0500 HST

To study the vertical structure of the Maui vortex, north-south and east-west cross sections through the approximate center of the Maui vortex are constructed. The north-south cross section shows westerly reversed flow ($>2 m s^{-1}$) along the axis of the counter-rotating

vortices up to the 1.8-km level, with orographically enhanced easterly winds >9 and $11 m s^{-1}$ along the northern and southern coasts, respectively (Fig. 9a). At the lowest levels ($<300 m$) over the Central Valley, weak ($\sim 1 m s^{-1}$) easterly katabatic flow, originating from the leeside lower slopes of Haleakala, is evident (Fig. 9a). The presence of a cyclonic-anticyclonic couplet, extending upward to the approximate base of the trade wind inversion, is also evident ($\sim 1.8 km$; Fig. 9b). At the lowest levels, the axis of the cyclonic (anticyclonic) maximum is displaced northward (southward; Fig. 9b) due to the presence of katabatic flow from the leeside slopes of Haleakala (Fig. 9a). The largest cyclonic (anticyclonic)

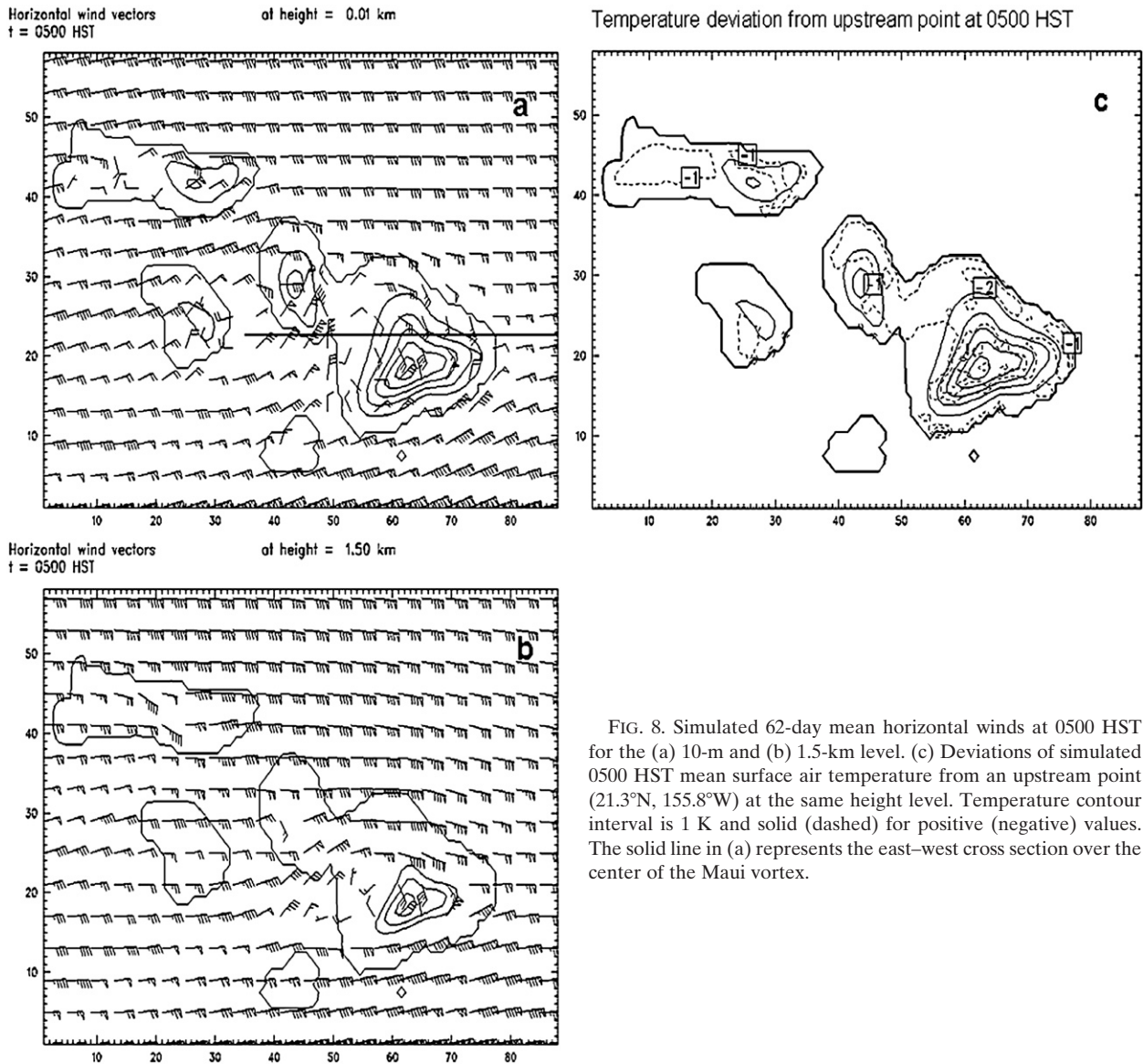


FIG. 8. Simulated 62-day mean horizontal winds at 0500 HST for the (a) 10-m and (b) 1.5-km level. (c) Deviations of simulated 0500 HST mean surface air temperature from an upstream point (21.3°N, 155.8°W) at the same height level. Temperature contour interval is 1 K and solid (dashed) for positive (negative) values. The solid line in (a) represents the east–west cross section over the center of the Maui vortex.

shear in low levels occurs along the northern (southern) coast between the strong easterly winds offshore and the weak katabatic flow over the Central Valley. The equivalent potential temperature exhibits a minimum along both the northern and southern coasts (Fig. 9d), indicative of descending airflow and a weak hydraulic jump behind the convex shape of the coastline (Fig. 1) as the strong ($>9 \text{ m s}^{-1}$) easterly winds move over the coastal mountain ridges (Fig. 9a). With nocturnal cooling and weak sinking motion at night (Fig. 9c), the simulated equivalent potential temperature over the Central Valley, in the lowest 1 km, is about 2 K lower than over the adjacent ocean (Fig. 9d).

The east–west cross section shows that the katabatic flow is the deepest over the Central Valley and is very

shallow on the leeside slopes of Haleakala where the westerly reversed flow ($<1 \text{ m s}^{-1}$) is simulated above the surface (Fig. 10a). A shallow nocturnal inversion is evident in the lowest levels immediately above the land surface (Fig. 10b). Above the trade wind inversion ($\sim 2 \text{ km}$), strong ($>9 \text{ m s}^{-1}$) downslope winds are simulated to the lee of Haleakala, with a hydraulic jump (Fig. 10a). The simulated equivalent potential temperature contours aloft (Fig. 10b) tilt downward, with sinking motion in the lee followed by an abrupt jump, with rising motion (Fig. 10c) and upward tilt of the contours. The relative humidity contours (Fig. 10d) also show that relatively drier air above the trade wind inversion was brought downward in the lee followed by the upward tilt of a moist tongue associated with the jump. Wave breaking, with hydraulic jump

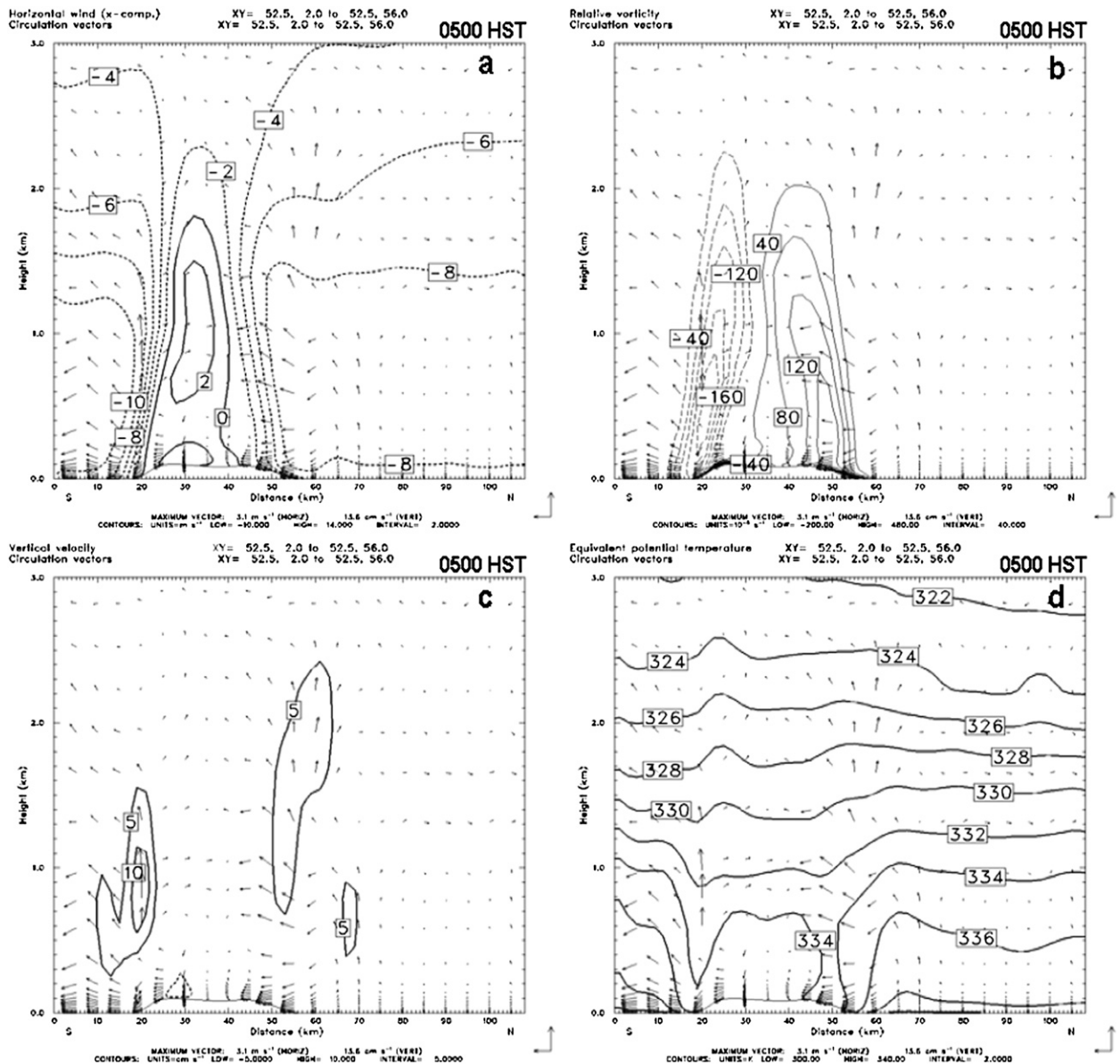


FIG. 9. Simulated 62-day north-south vertical cross section (Fig. 6a) at 0500 HST for (a) the u -wind component (every 2 m s^{-1}), (b) relative vorticity (every $40 \times 10^{-5} \text{ s}^{-1}$), (c) vertical velocity (every 5 cm s^{-1}), and (d) equivalent potential temperature (every 2 K).

features, is also evident in the lee of the West Maui Mountains.

7. Airflow at 1400 HST

a. Horizontal view

At the surface, anabatic/upslope trade wind flow prevails over much of the windward northeastern and southeastern slopes of Haleakala (Fig. 11a). Flow deceleration and flow splitting on the windward side of Haleakala

are less significant at 1400 HST than at night, with an onshore wind component on the eastern windward side of Haleakala. The simulated daytime surface flow in the lee sides of Haleakala and West Maui is dominated by sea-breeze/upslope flow. The Maui vortex is joined by a weak southern anticyclonic vortex as the westerly return flow merges with the daytime upslope flow ($< 4 \text{ m s}^{-1}$) on the leeside lower slopes of Haleakala (Fig. 11a). As a result, both the Maui vortex and the southern anticyclonic vortex at the surface are more significant as compared with the nighttime flow.

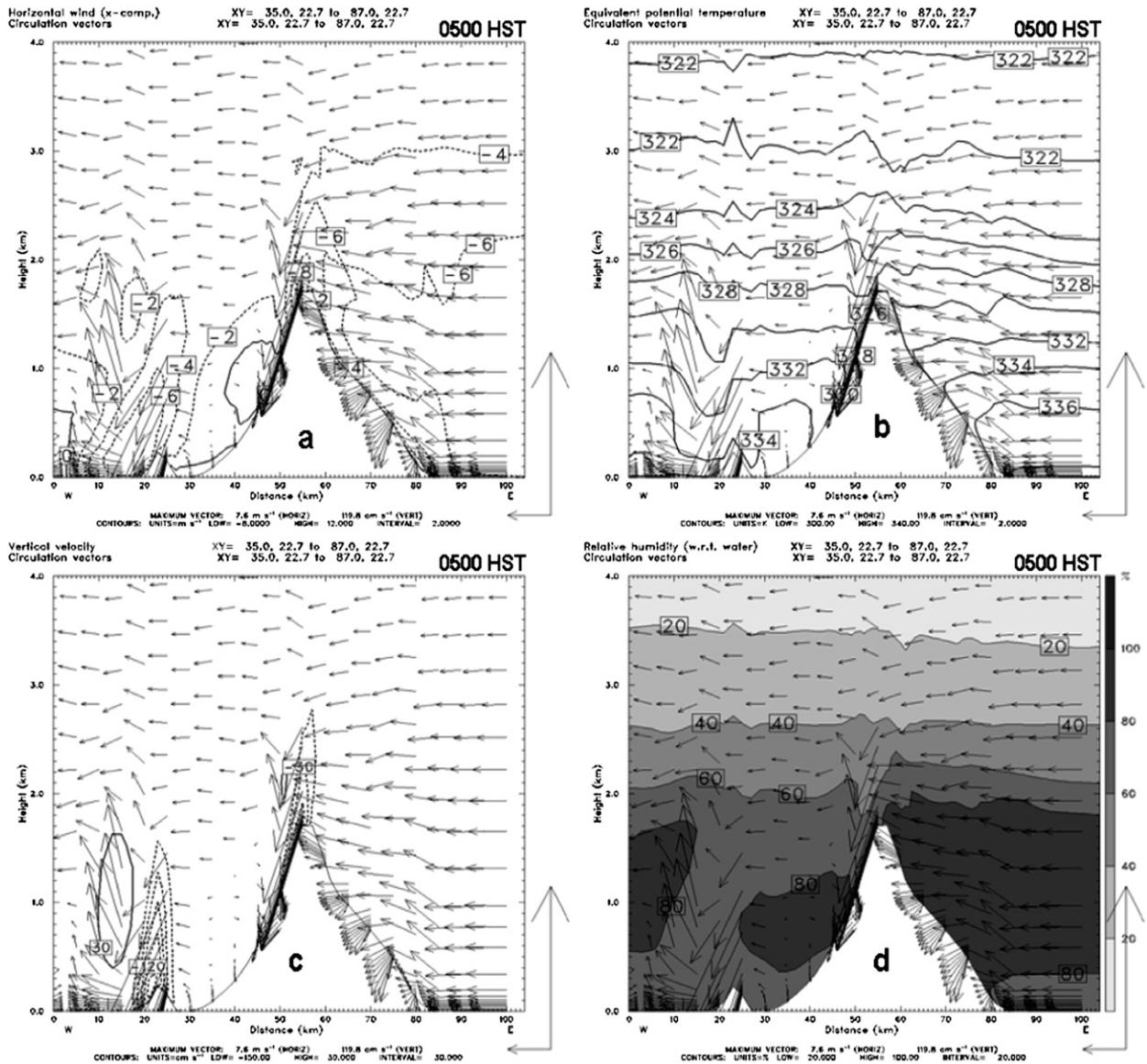


FIG. 10. Simulated 62-day mean east–west cross section (Fig. 8a) at 0500 HST for (a) the u -wind component (every 2 m s^{-1}), (b) equivalent potential temperature (every 2 K), (c) vertical velocity (every 30 cm s^{-1}), and (d) relative humidity (every 20%).

Over the West Maui Mountains, the simulated daytime surface flow shows the combined onshore–trade wind flow on the windward side (Fig. 11a). Near Kahului, daytime onshore flow combined with deflected trade wind flow results in strong winds (8 m s^{-1}) (Fig. 11a) compared to the mean state (6 m s^{-1}) (Fig. 5a) and nighttime (4 m s^{-1}) (Fig. 8a) flows. The locally strong winds in the afternoon hours, especially under strong trades, may adversely affect aviation traffic to the nearby Kahului Airport. With afternoon solar heating, the downslope winds on the southeastern leeside slopes of West Maui and the Ma’alaea Bay region are less significant than at night because of weaker orographic blocking. With much

weaker northeasterly winds from the southeastern foothills of the West Maui Mountains (Fig. 11a) than at night (Fig. 8a), the westerly onshore/upslope flow extends off the southwestern leeside coastline of the Central Valley. As a result, the Maui vortex at the surface (Fig. 11a) has a larger east–west horizontal extent than at night (Fig. 8a). In the lee side of West Maui, the model simulates an anticyclonic lee vortex at the surface between the northeasterly flow on the eastern flank of the West Maui Mountains and the combined return/onshore flow along the leeside coast. Cyclonic shear is evident off the northern leeside coast between the gap winds ($\sim 11 \text{ m s}^{-1}$) and the combined westerly onshore/upslope flow in the lee of the

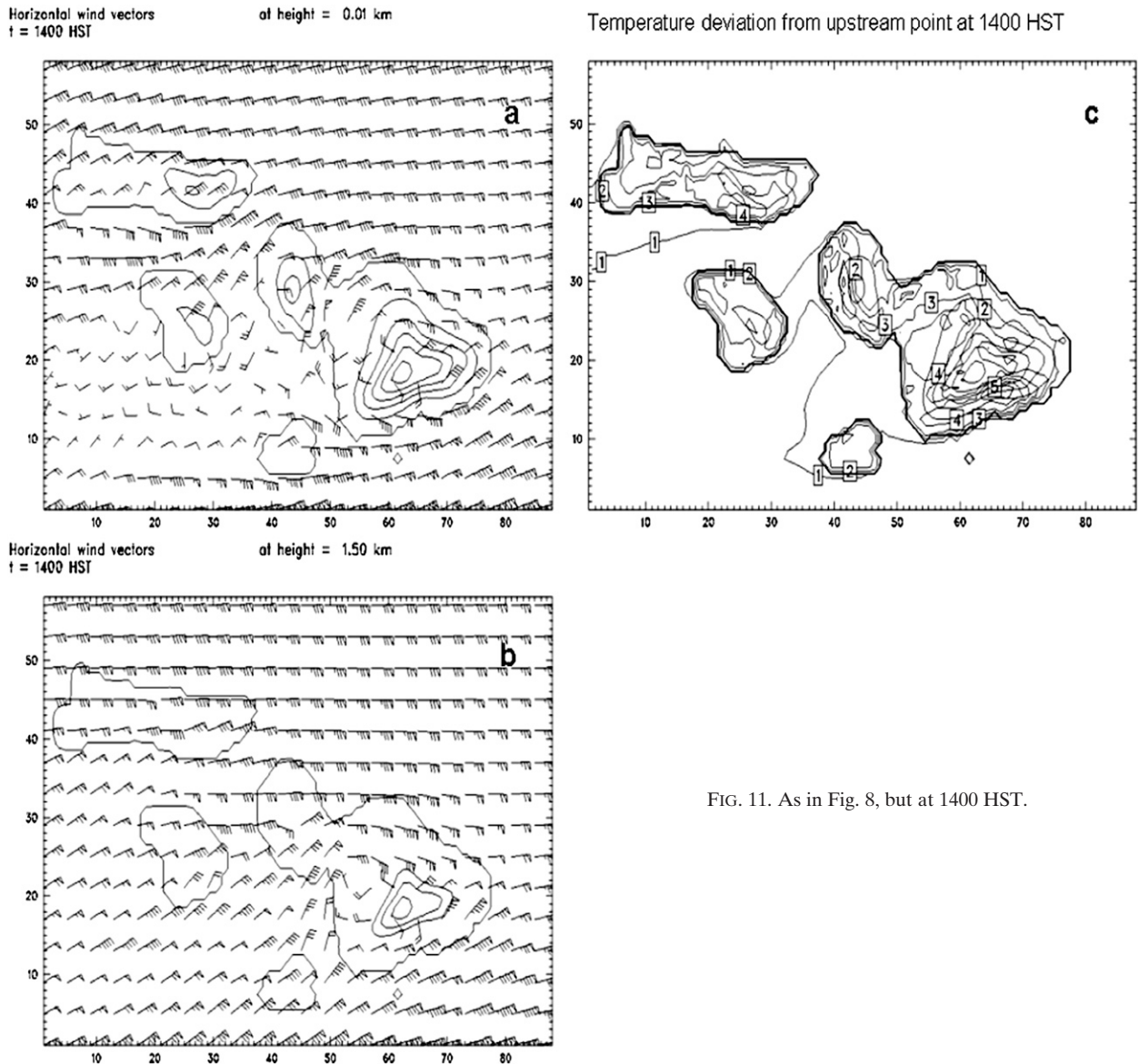


FIG. 11. As in Fig. 8, but at 1400 HST.

West Maui Mountains. Over Molokai, a sea-breeze convergent line is simulated inland along the southern coast of eastern Molokai.

Similar to the island of Hawaii (Chen and Wang 1994), the largest positive daytime temperature anomalies (>5 K) occur in the semiarid leeside areas, with ridge tops below the trade wind inversion, including the southeastern slopes of Haleakala, the southeastern leeside areas of the West Maui Mountains, and the southern leeside slopes of Molokai (Fig. 11c). The western leeside slopes of Haleakala also have relatively large warm anomalies (>4 K), with a local maximum behind the northern ridge axis of Haleakala. The smallest warm anomalies (<2 K) occur on the northern windward sides of Haleakala and

the West Maui Mountains, with frequent showers and persistent orographic lifting. These areas are covered by a tropical rain forest.

One of the striking differences between daytime and nighttime airflows occurs over the coastal waters. Westerly reversed flow develops in the wake zones off the Maui and Lanai leeside coasts in the afternoon and extends more than 40 km downstream (Fig. 11a). Winds along the northern and southern coasts of Haleakala, and within the ocean channel between West Maui and Molokai (Fig. 11a), are also slightly stronger as compared with the nighttime flow (Fig. 9a). Nguyen et al. (2010) studied the airflow in the wake zone off the western leeside coast of Oahu. Despite its relatively small size

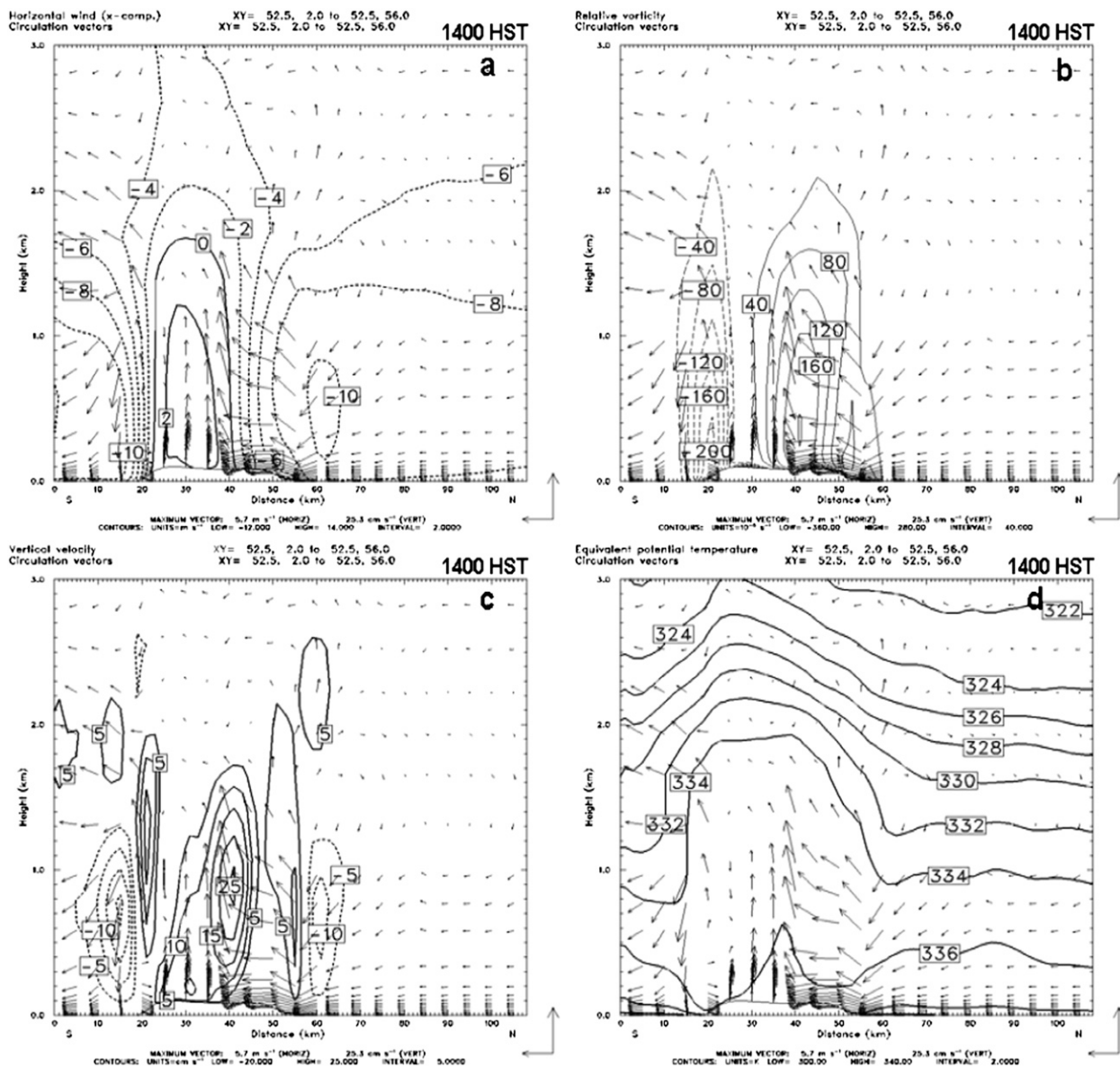


FIG. 12. As in Fig. 9, but at 1400 HST.

(with a horizontal dimension ~ 45 km), they found that thermal forcing over the island plays a significant role in the flow reversal within the leeside wake zone offshore during the daytime. The impact of daytime heating on airflow and the Maui vortex will be discussed further in section 10 based on model sensitivity tests.

Above the surface, the winds over the channels at the 1.5-km level are stronger than the nighttime flow, with wind speeds approximately 13 m s^{-1} over a large area of the Alenuihaha Channel and a small region of the Pailolo Channel (Fig. 11b). At the 1.5-km level, in contrast to the surface, the east–west horizontal extent of the lee vortices is slightly smaller than at night (15 versus 24 km)

with a slightly weaker westerly return flow aloft (Figs. 11b and 8b).

b. Vertical structure of the Maui vortex at 1400 HST

The westerly reversed flow ($1\text{--}2 \text{ m s}^{-1}$), with rising motion over the Central Valley, extends from the surface up to the 1.6-km level (Fig. 12a). The rising motion ($\sim 25 \text{ cm s}^{-1}$) is mainly a result of daytime heating and convergence along the axis of the counter-rotating eddies (Fig. 12c). The axis of maximum vorticity is located over the Central Valley (Fig. 12b) between the westerly return/upslope flow and strong easterly winds along the northern coast, whereas the axis of the anticyclonic maximum is

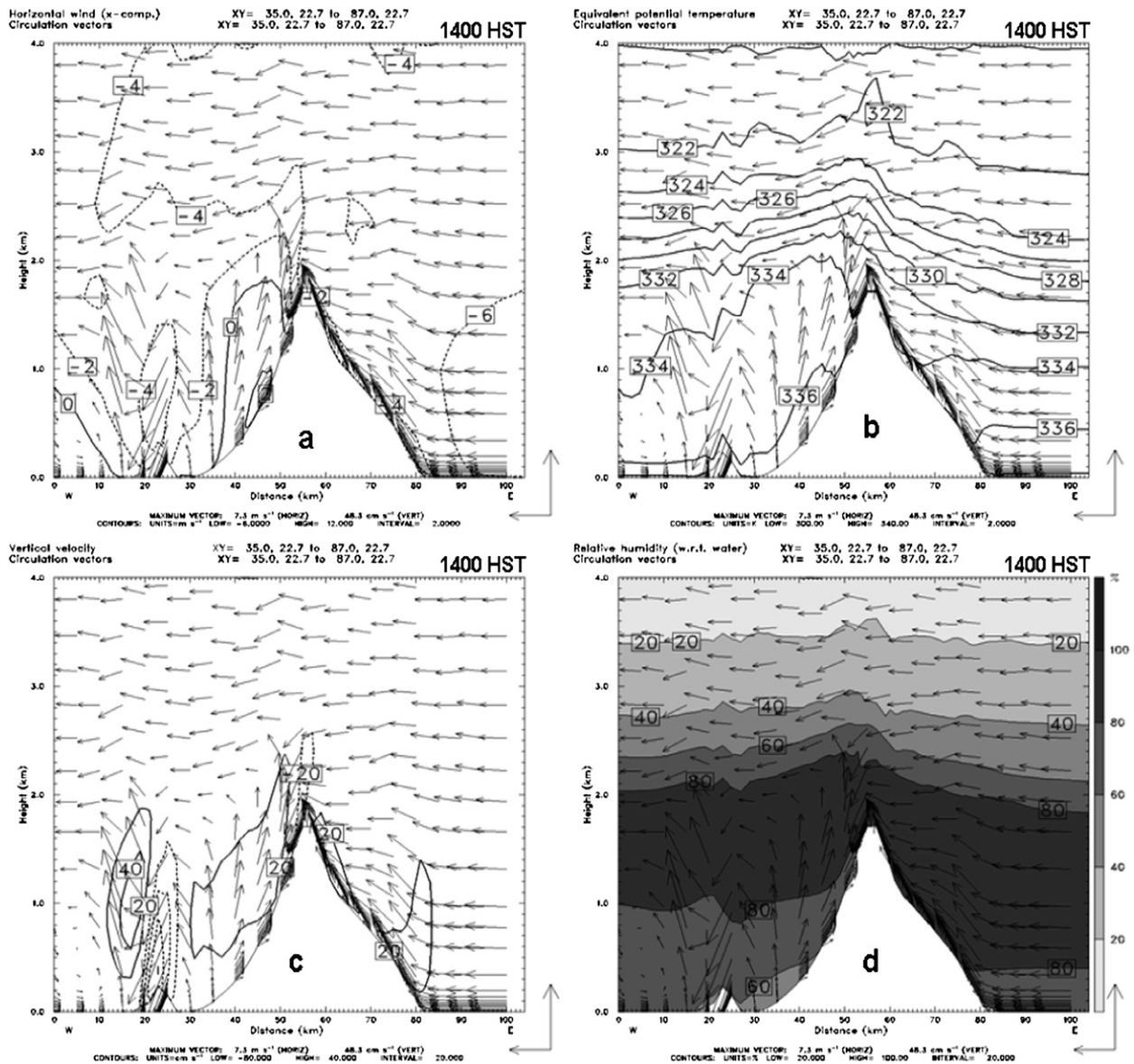


FIG. 13. As in Fig. 10, but at 1400 HST. Contour intervals are 2 m s^{-1} , 2 K , 20 cm s^{-1} , and 20% , respectively.

over the southern coast (Fig. 12b). The equivalent potential temperature over land is rather uniform vertically, with the 334-K contour line extending above the 1.6-km level (Fig. 12d); and the values in low levels are less than the open ocean (336 versus $>338 \text{ K}$) because of vertical mixing initiated by solar heating. Above the surface layer, the rising motion over the Central Valley (Fig. 12c) brings the low-level, high equivalent potential temperature air upward (Fig. 12d). It is apparent that because of vertical motions, the trapping of pollutants over the Central Valley by the vortex circulation would be less significant in the afternoon than at night even though the vortex circulation at the surface is more pronounced.

The equivalent potential temperature minima at the northern and southern coast (Fig. 12d) are indicative of a hydraulic jump behind the ridges associated with the concave coastline.

Above the trade wind inversion, the downslope flow to the lee of Haleakala is weaker than at night (4 versus 8 m s^{-1} ; Figs. 10a and 13a), with a much weaker hydraulic jump. High equivalent potential temperature air is brought upward by the upslope flow in the lee converging with the descending drier airflow moving over the top of Haleakala (Fig. 13b). A weak hydraulic jump is evident on the southern leeside slopes of the West Maui Mountains, with drier, low equivalent potential

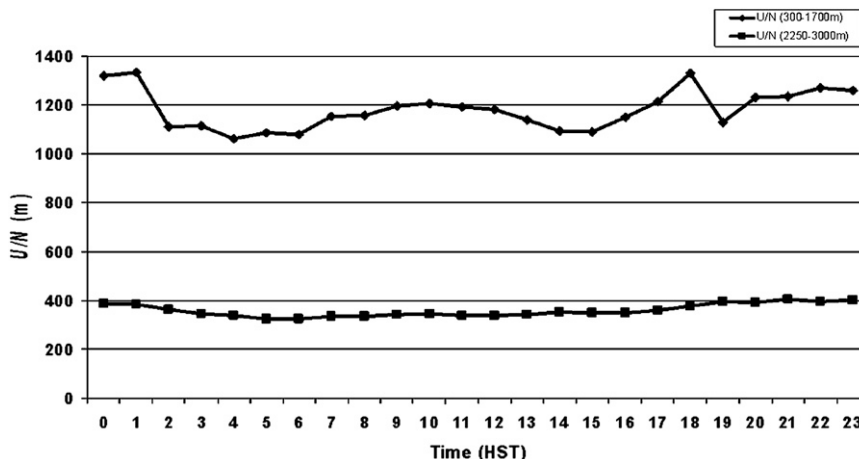


FIG. 14. 62-day mean diurnal variations of layer mean U/N for the layers between 300 and 1700 m, and between 2250 and 3000 m for an upstream point (21.3°N , 155.8°W).

temperature air descending from aloft in the lee followed by abrupt ascent (Figs. 13b,d). However, with daytime heating, the easterly downslope wind component on the leeside slopes of the West Maui Mountains is much weaker than the nighttime flow, followed by weak combined onshore/return flow off the leeside coast (Fig. 13a).

For theoretical studies of airflow past a 3D barrier, N is frequently considered as independent of height ($\sim 1 \times 10^{-2} \text{ s}^{-1}$). For the trade wind flow, the stability (N) varies considerably with respect to height. In low levels, N is about $0.4 \times 10^{-2} \text{ s}^{-1}$ because of fluxes from the ocean surface and vertical mixing. Air becomes more stable above and N increases to about $1.4 \times 10^{-2} \text{ s}^{-1}$ below the trade wind inversion. The U/N for the 300–1700-m layer and the 2250–3000-m layer above the trade wind inversion are about 1200 and 400 m, respectively (Fig. 14). For the West Maui Mountains, h (~ 1700 m) is greater than U/N (~ 1200 m). For Haleakala, the difference between mountain height and trade wind inversion is about 1000 m, which is much greater than U/N aloft (~ 400 m). Thus, wave breaking and a hydraulic jump occur over the West Maui Mountains and leeside slopes of Haleakala as shown in our model simulations. Since the trade wind inversion is not a rigid surface, air above the trade wind inversion could descend to low levels in the lee. With $h > U/N$, flow deflection is also simulated on the windward side of West Maui, especially at night. The diurnal variations in U/N over the open ocean are relatively small (Fig. 14) and are mainly related to slightly stronger winds aloft after sunset. The main differences in nighttime and daytime flow regimes are related to changes in stability and thermally driven diurnal flows over land.

8. Transition periods

In this section, the evolution of the surface airflow during the early morning and evening transitions is examined from the north–south cross-sectional plots through the valley and east–west cross-sectional plots along the approximate axis of the westerly return flow in the lee of Haleakala. The focus is on the change in airflow in response to land surface heating and cooling.

a. Morning transition

Sunrise during the months of July and August 2005 ranged from 0553 local time at the start of July to 0615 local time by the end of August. At 0600 HST, the horizontal surface flow over Maui (not shown) is very similar to the surface airflow at 0500 HST (Fig. 8a). The simulated morning transition begins after sunrise as the katabatic flow on the leeside slope of Haleakala transforms to weak anabatic winds before 0700 HST (Figs. 15a,b). The westerly reversed flow in the lee above the surface weakens to $\sim 2 \text{ m s}^{-1}$ (Fig. 15b). At the same time, the nocturnal inversion along the leeside slopes of Haleakala is disappearing (Fig. 15c). Above the trade wind inversion on the leeside slopes of Haleakala, the downslope flow and the hydraulic jump weaken after sunrise (Figs. 15b and 16b). On the southeastern and northeastern slopes of Haleakala, winds start to turn after sunrise, with an upslope wind component at 0700 HST (Fig. 15a).

On the western leeside slopes of Haleakala, the westerly return flow above the surface continues to weaken, whereas the upslope flow along the leeside slope surface continues to strengthen in response to the development of a daytime thermally driven circulation above the leeside

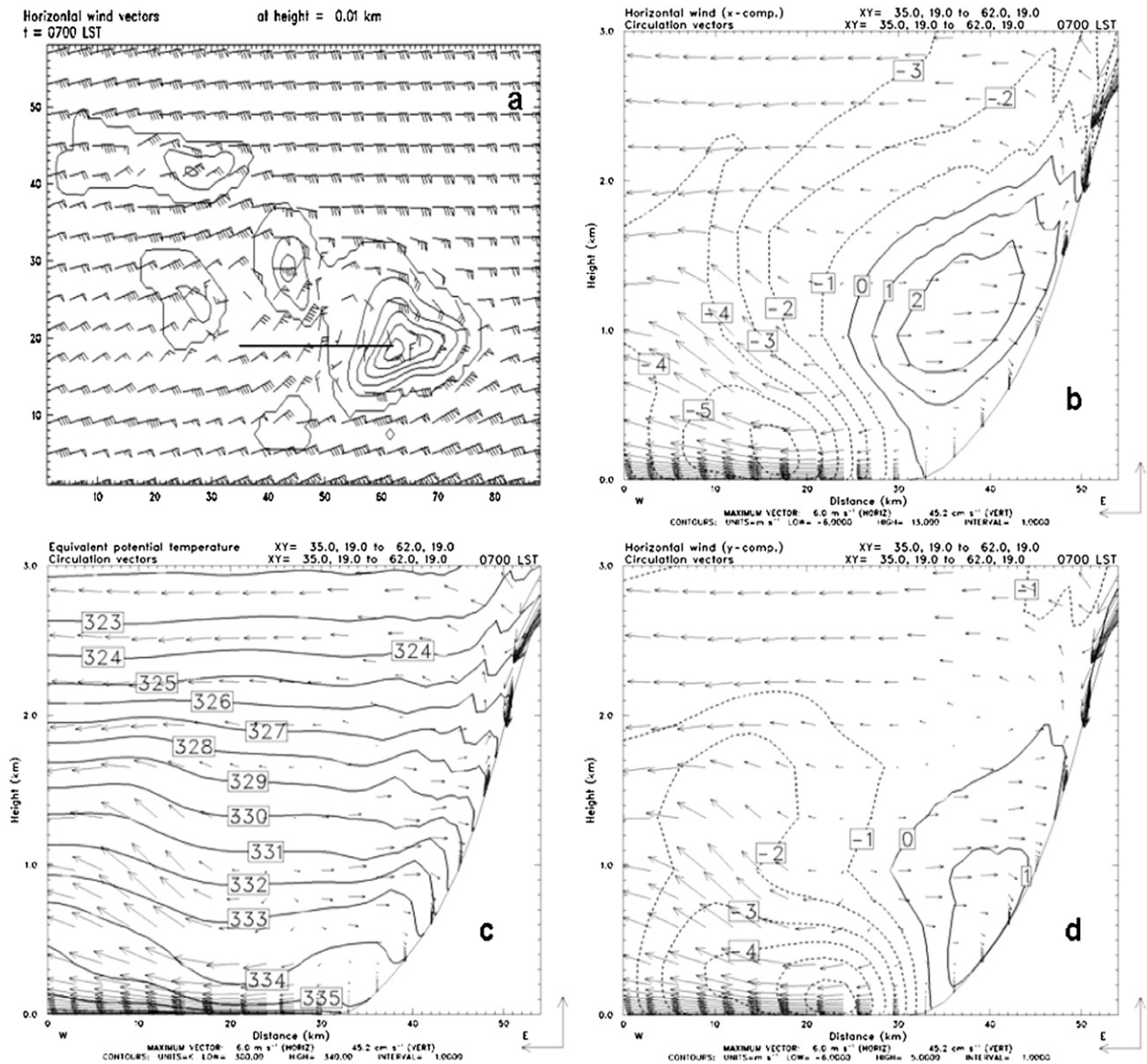


FIG. 15. (a) Horizontal surface winds, and a new east–west cross section of the (b) u -wind component (every 1 m s^{-1}), (c) equivalent potential temperature (every 2 K), and (d) v -wind component (1 m s^{-1}) at 0700 HST. The east–west cross section shown in (a) is along the approximate axis of the westerly return flow.

slopes (Fig. 16b). Shifting of surface flow from a downslope wind to an upslope wind component over Haleakala is completed around 0800 HST (Fig. 16a). With calm mean winds, relatively clear skies, dry soils, and semiarid ground cover, the turning from katabatic to anabatic flow on the lee side of Haleakala is relatively short in comparison with the windward side of the island of Hawaii (Chen and Nash 1994), and is completed in less than 2 h.

The windward side of the West Maui Mountains exhibits a downslope wind component on the southern foothills at 0600 HST (not shown). The wind shifts to a combined upslope/deflected trade wind flow by

0800 HST (Fig. 16a). With the onset of daytime heating, strong northerly winds from the southeastern foothills of West Maui and leeside downslope winds over the top of the mountain begin to decrease after sunrise (Figs. 15a and 16a). The West Maui lee vortices move closer to the West Maui Mountains concurrent with the transformation of the offshore/downslope flow to sea-breeze/upslope flow on the lee side.

b. Evening transition

The western lee side of Haleakala is dry (Giambelluca et al. 1986). Without significant rain evaporative cooling

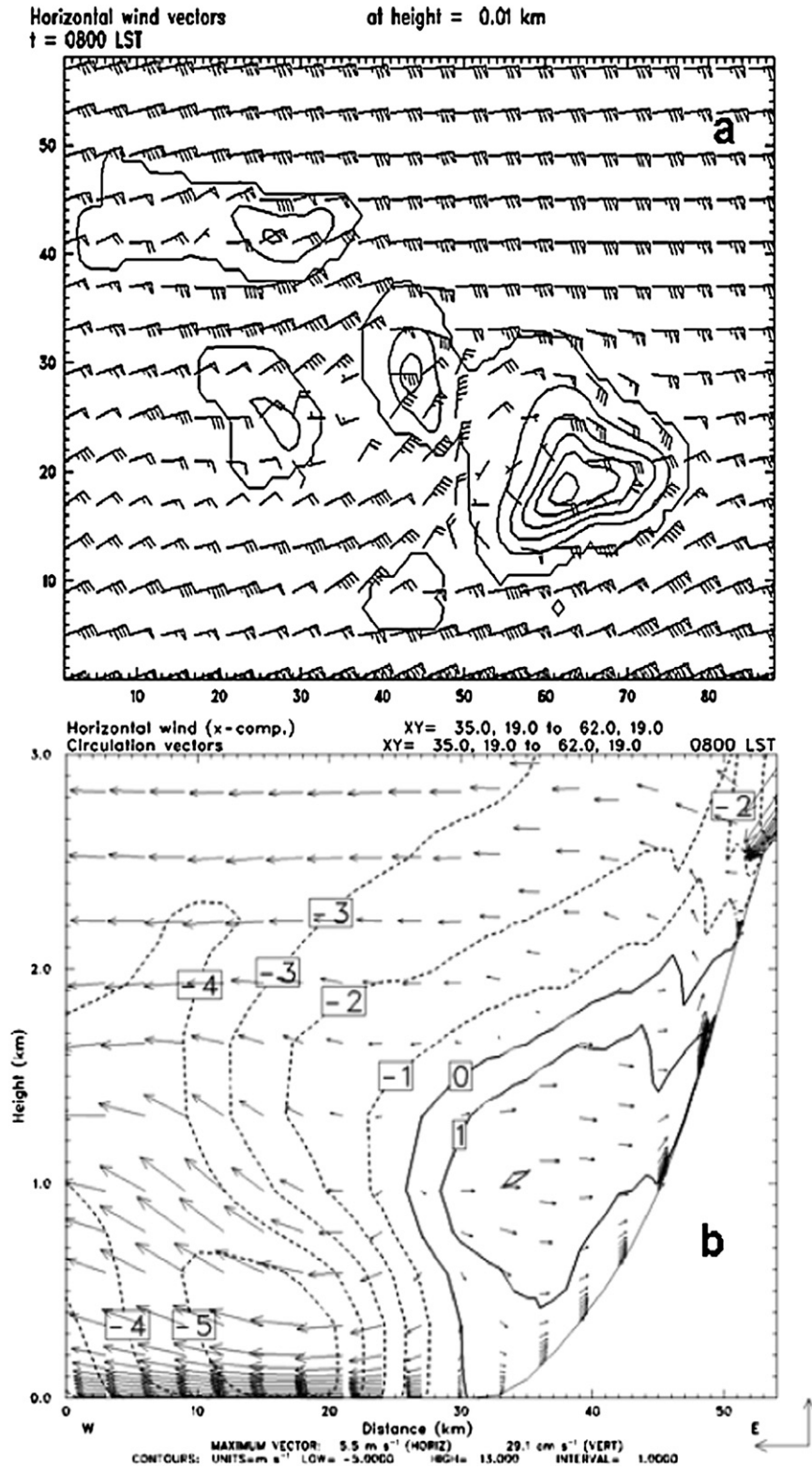


FIG. 16. (a) Horizontal surface winds and (b) the east–west cross section (Fig. 15a) of the u -wind component (every $1 m s^{-1}$) at 0800 HST.

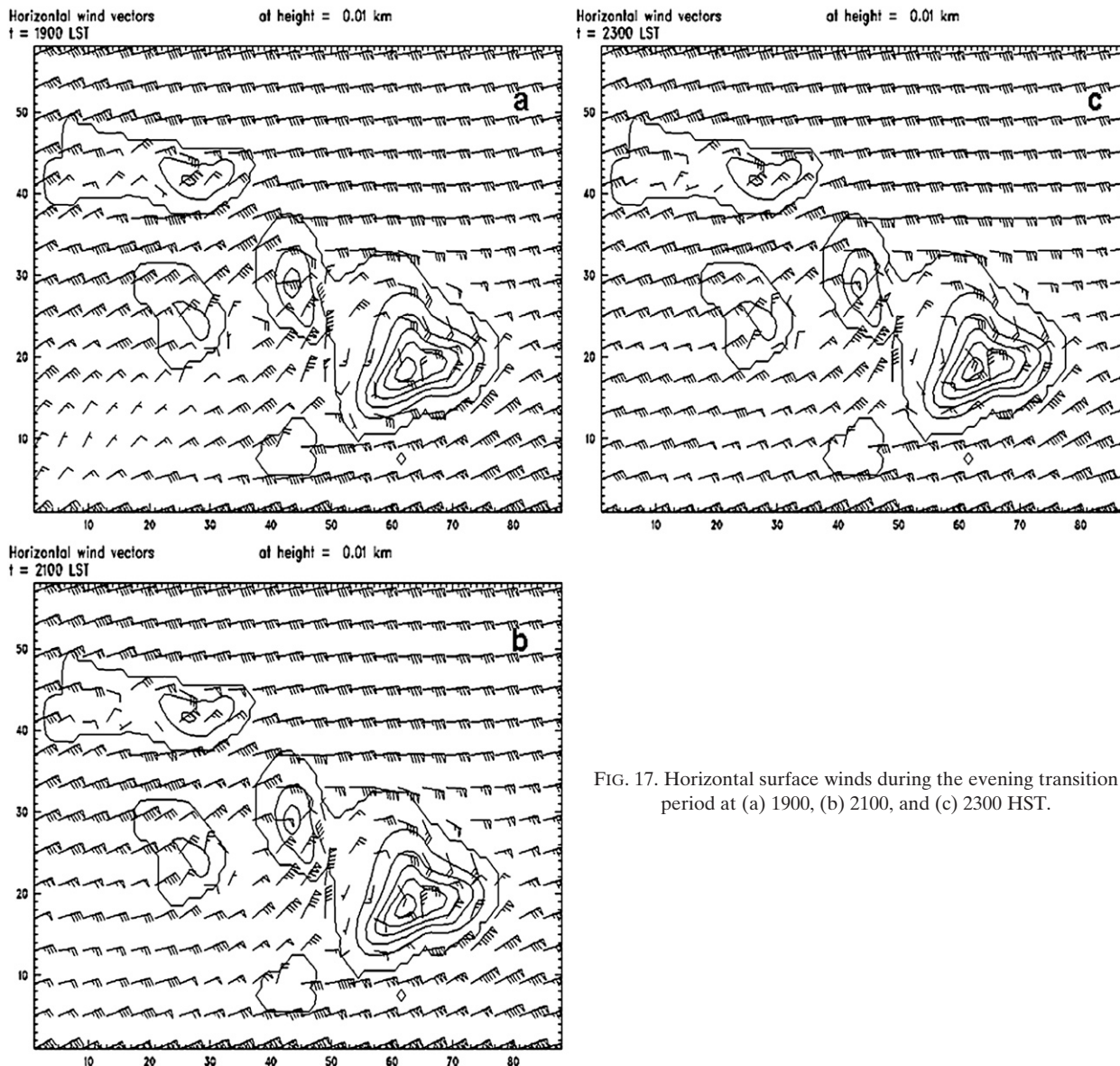


FIG. 17. Horizontal surface winds during the evening transition period at (a) 1900, (b) 2100, and (c) 2300 HST.

and without the presence of a steep land–sea boundary, the evening transition, driven mainly by nocturnal cooling, is a relatively slow process as compared with the windward Hilo Bay area and the leeside coast of the island of Hawaii (Chen and Nash 1994).

At 1900 HST, katabatic winds start to develop at the 0.8-km elevation (Fig. 18a), with the forming of a nocturnal inversion immediately above the surface (not shown). Above the trade wind inversion, strong downslope winds on the upper leeside slopes develop (Fig. 18a). In the mean time, orographic blocking by the West Maui Mountains becomes more significant than earlier, with strong low-level northeasterly winds off the southwestern coast of the Central Valley. Westerly downslope flow develops

on the eastern windward side of Haleakala as a combined effect of land surface cooling and orographic blocking (Figs. 17a–c). With continued land surface cooling, the katabatic winds progress downward toward the Central Valley. Concurrently, the downslope winds along the upper slope of Haleakala increase (Figs. 18a,b). By 2300 HST, the katabatic winds extend to the western leeside foothills of Haleakala (Fig. 18c). The westerly return flow above the surface continues to increase. The disappearance of surface westerly winds over the Central Valley occurs after midnight. This is in contrast to the Kona lee side where the evening transition is completed before 2000 HST (Chen and Wang 1994).

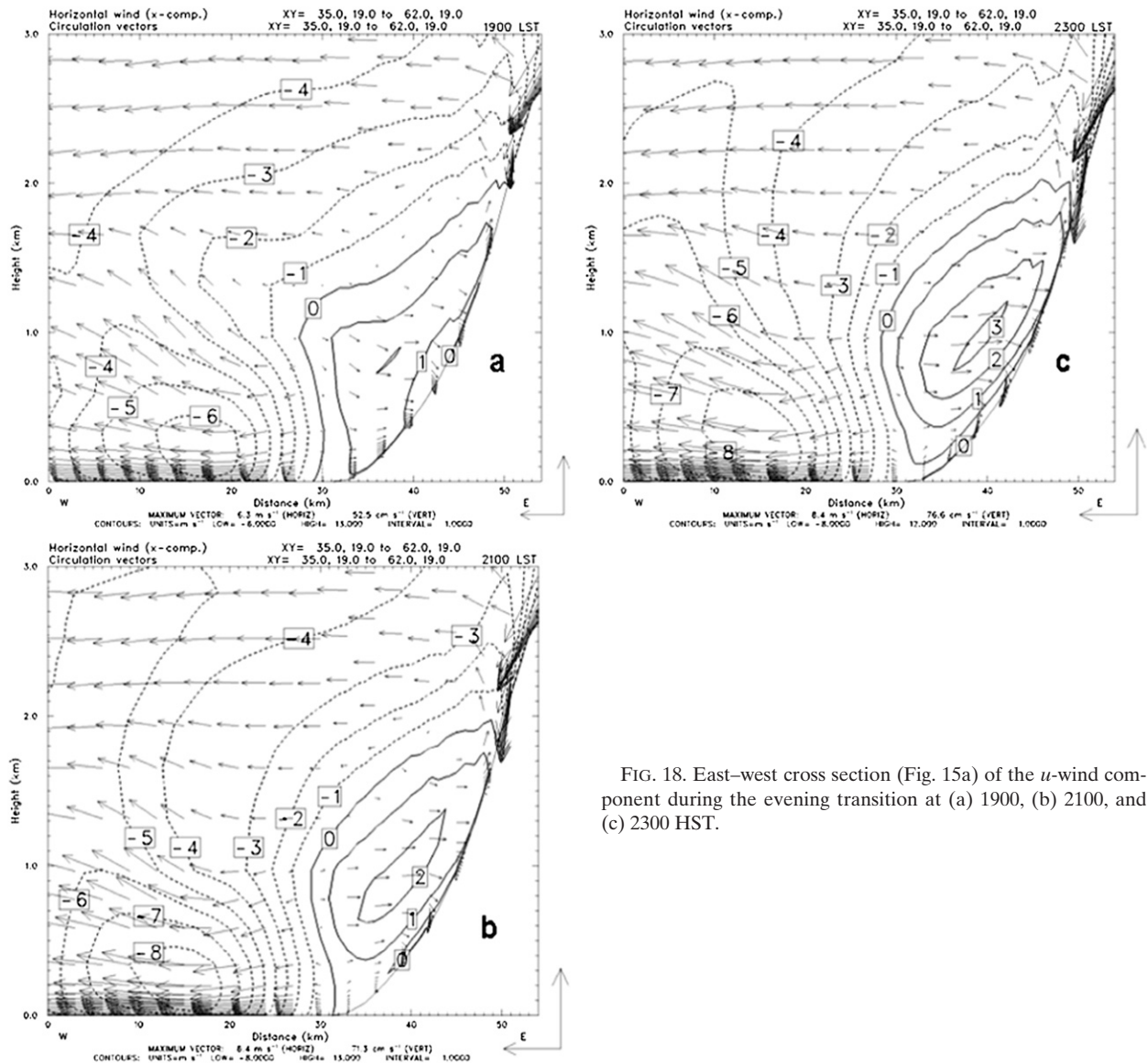


FIG. 18. East–west cross section (Fig. 15a) of the u -wind component during the evening transition at (a) 1900, (b) 2100, and (c) 2300 HST.

9. Impact of trade wind strength on the Maui vortex

At the surface, the deflection of the airflow by the convex shape of the terrain associated with the ridge axis along the northern coast of Haleakala is more significant for weak trades (Figs. 19a,b) than strong trades (Figs. 19c,d). For strong trades, the airflow tends to move over and down the ridge axis. As a result, the location of the circulation center of the Maui vortex is slightly to the south for strong trades compared to weak trades. On the windward side of the West Maui Mountains, the flow deflection is slightly more significant for weak trades than for strong trades. The Maui vortex is closer to the leeward foothills of Haleakala for weaker trades. For weak trades, the southern anticyclonic vortex does not

have a closed circulation (Fig. 19b). At the 1.5-km level, the vortices are more pronounced, westerly return flow is stronger, and the vortices extend farther downstream under stronger trades (Fig. 19d).

When trades are stronger, stronger downslope winds are simulated above the leeward slopes of Haleakala, followed by a more significant hydraulic jump above the trade wind inversion (not shown). The same is true in the lee of the West Maui Mountains. The westerly return flow in the lee of Haleakala is stronger for strong trade winds than for weak trades (3 versus 1 $m s^{-1}$; Figs. 20a,c). The zonal winds along the southern coast reach as high as 14 $m s^{-1}$ for strong trades as compared to 9 $m s^{-1}$ for weak trades. The north–south cross section shows a more significant cyclonic–anticyclonic couplet extending well

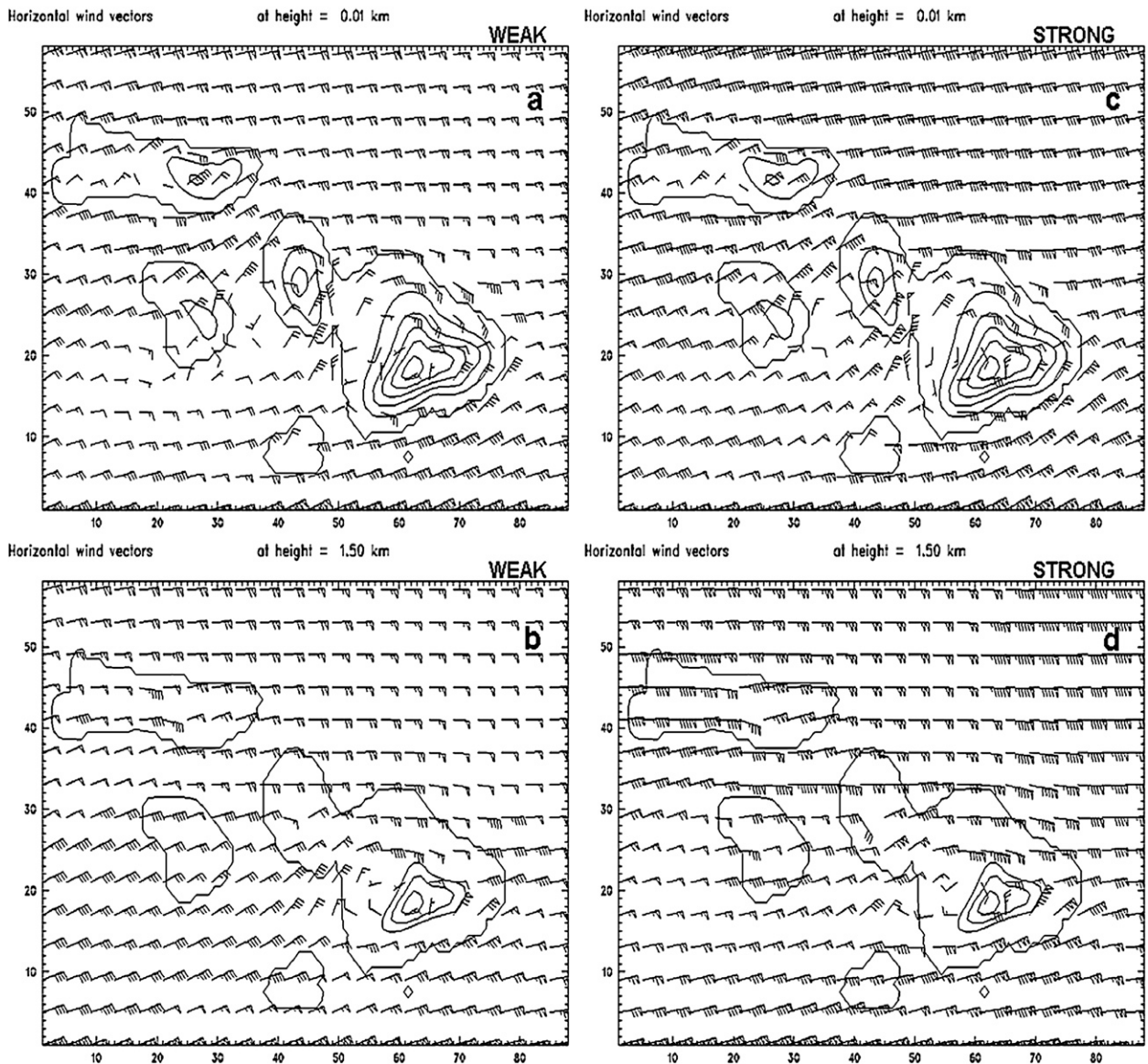


FIG. 19. Mean surface winds for the (a) six weak trade wind days and (c) six strong trade wind days. (b),(d) As in (a),(c), but for the 1.5-km level.

above the trade wind inversion when trades are stronger (Figs. 20b,d).

10. Effects of solar heating, latent heat release, and surface friction on the Maui vortex

Since our results suggest that the Maui vortex and airflow over the coastal waters are modified by land surface heating, a model sensitivity test is performed by reducing the solar constant by 50% (SOLAR). In the SOLAR run, the daytime maximum temperature deviations in the leeside areas reduce to 2–4 K (Fig. 21a) as compared to 4–6 K in the CTRL run (Fig. 21b). The

upslope flow over the northern, southern, and western lee slopes of Haleakala, with a closed circulation over the Central Valley are still evident (Fig. 21c). However, in the SOLAR run, the orographic blocking on the windward side of the West Maui Mountains is more significant; the Maui vortex has a larger north–south extent with its center shifting southward as compared to the CTRL run (Figs. 21c,d). Within the wake zone off the Maui leeside coast, the westerly reversed flow, extending to more than 40 km downstream, still exists but with weaker wind speed as compared to the CTRL run (2–4 versus 3–5 m s^{-1} ; Figs. 21c,d). With reduced solar heating, both the cyclonic circulation associated with the Maui

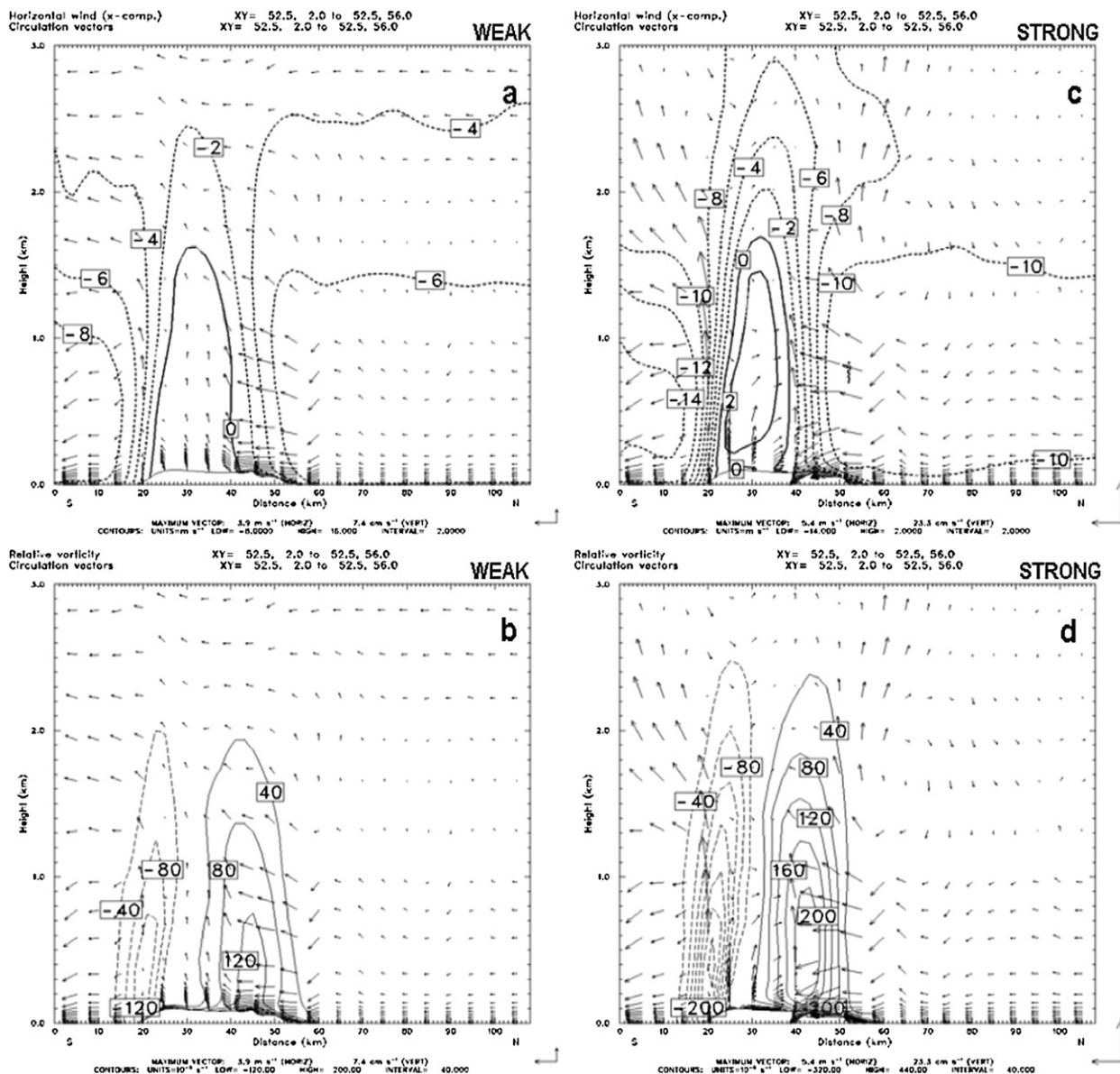


FIG. 20. North–south cross section (Fig. 6a) of the mean u -wind component (2 m s^{-1}) for the (a) weak and (c) strong trade wind days. (b),(d) As in (a),(c), but for relative vorticity (every $40 \times 10^{-5} \text{ s}^{-1}$).

vortex and the southern anticyclonic vortex to the south, at the surface, are weaker. On the other hand, the flow deflection by the West Maui Mountains becomes more significant, with stronger northerly/northeasterly flow along the western leeward coast of Haleakala (Fig. 21e). An anomalous convergence line in the SOLAR run is present off the eastern windward coast of Haleakala because of more significant flow deceleration upstream and weaker upslope flow over the windward slopes (Fig. 21e). The weaker westerly flow in the wake zones off the leeward coasts of Maui and Lanai in the SOLAR run is accompanied by weaker winds around the corner

of the northern ridge axis of Haleakala, over the ocean channel between West Maui and Molokai, as well as over the coastal waters off the southeastern coast of Haleakala (Fig. 21e). In other words, the “channeling effects” are reduced with a weaker westerly flow in the wake zones off the Maui and Lanai leeward coasts. Furthermore, the intensity of the upslope/westerly return flow on the lee slopes of Haleakala is greatly reduced (Fig. 22a) as compared to the CTRL run (Fig. 22b).

A model sensitivity test is conducted by turning off the latent heat release in the model (NOLH; Fig. 23). Since

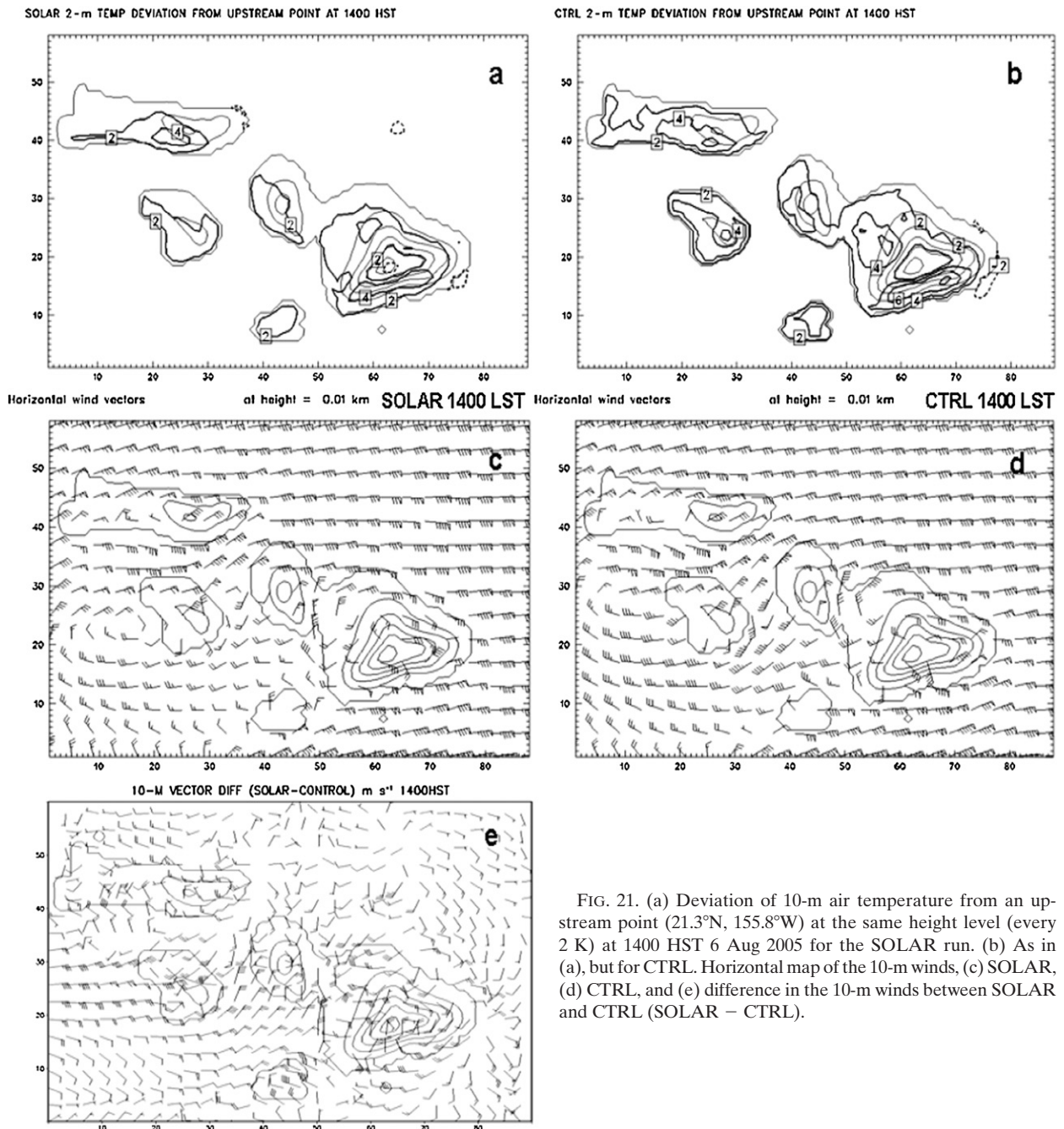


FIG. 21. (a) Deviation of 10-m air temperature from an upstream point (21.3°N, 155.8°W) at the same height level (every 2 K) at 1400 HST 6 Aug 2005 for the SOLAR run. (b) As in (a), but for CTRL. Horizontal map of the 10-m winds, (c) SOLAR, (d) CTRL, and (e) difference in the 10-m winds between SOLAR and CTRL (SOLAR - CTRL).

most of the rainfall and precipitation occurs over land as the trade wind cumuli interact with the island-induced airflow and terrain, latent heating mainly affects thermal fields over land (Fig. 23b). As a result, the impact of latent heating on surface airflow is qualitatively similar to the effects of reduced solar heating. The 24-h differences in surface wind vectors between the NOLH and CTRL runs (Fig. 23a) are similar to reduced solar heating (Fig. 21e) but with smaller magnitudes. Latent heat release also

affects the stability over the island. Below the 1.8-km level, the air is ~ 2 K colder with a more pronounced inversion layer (~ 2 km) for the NOLH run than the CTRL run (Figs. 24a,b). Above the 1.8-km level, with $h > U/N$, dual-counter-rotating vortices are present in the NOLH run with more significant orographic blocking on the windward side as compared to the CTRL run (Figs. 23c,d). The dual-rotating vortices extend well above the mean 1.8-km level in the NOLH run (Figs. 24c,d).

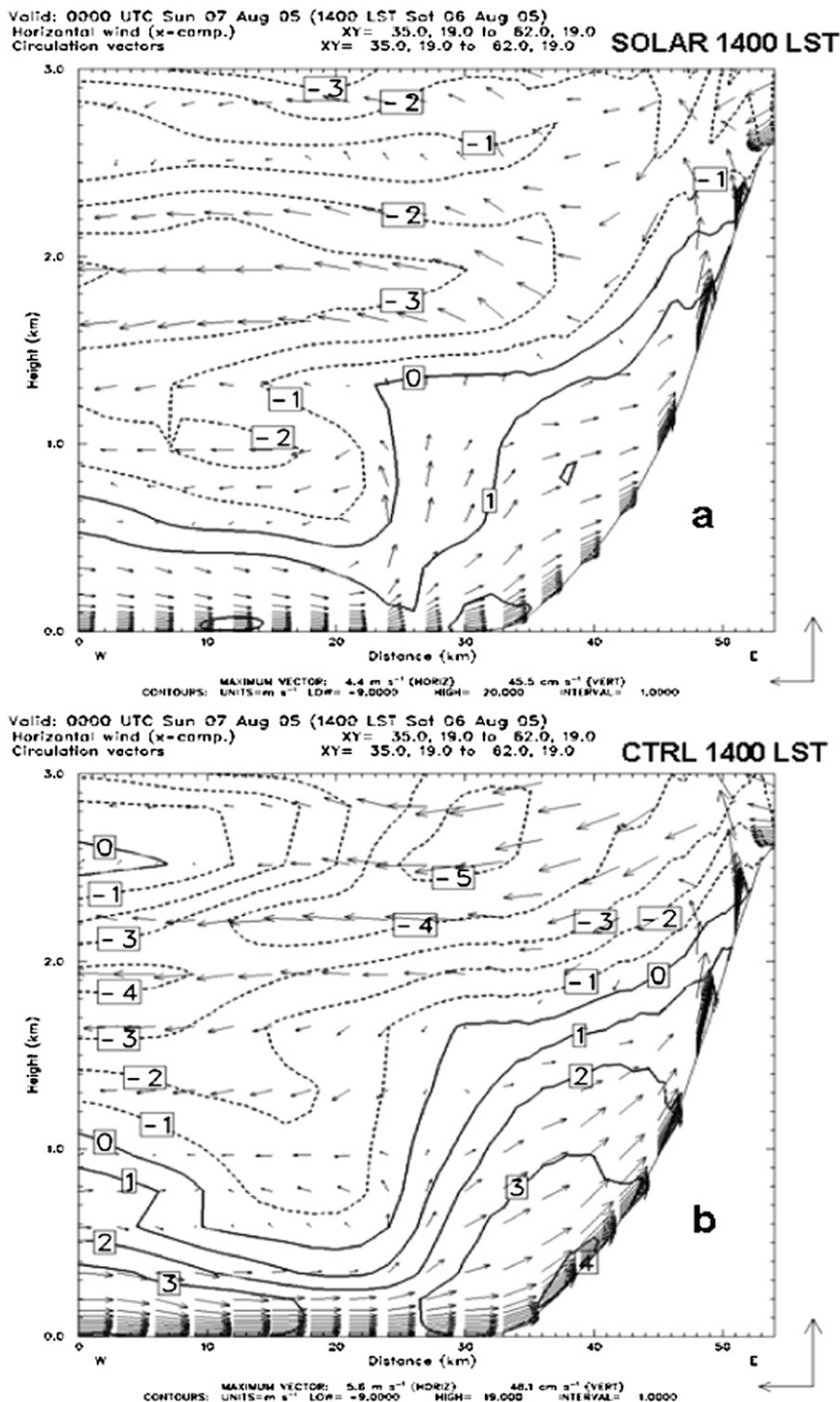


FIG. 22. East–west vertical cross section (Fig. 15a) of u -wind component (every 1 m s⁻¹) at 1400 HST 6 Aug 2005: (a) SOLAR and (b) CTRL runs.

Without surface friction (NOFR), because of stronger winds over land (Fig. 25a), the dual-rotating vortices to the lee of Haleakala (Figs. 25b,c) are very similar to the CTRL run (Figs. 7c,d), except the magnitudes are

larger near the surface (Figs. 25b,c). With stronger winds (>2–3 m s⁻¹) over land, especially along northeastern and southeastern flanks of Haleakala, orographic blocking on the windward side of the West Maui Mountains and

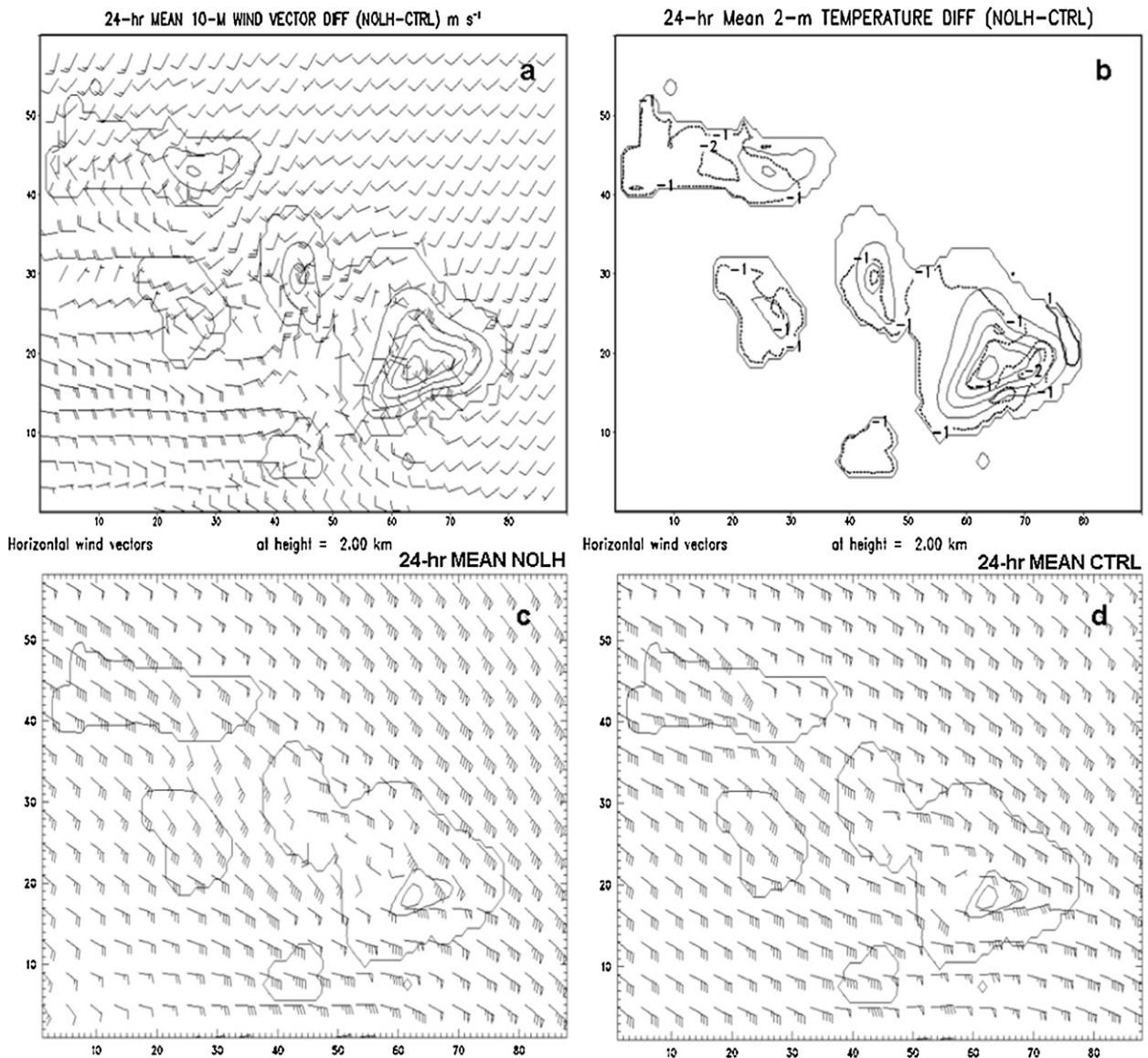


FIG. 23. 24-h mean from the NOLH run. (a) Differences in the surface winds between NOLH and CTRL (NOLH – CTRL) for Maui County, (b) 24-h mean 2-m temperature difference (NOLH – CTRL) with solid (positive) and dashed (negative) contours (every 1 K), (c) winds at the 2-km level for the NOLH run, and (d) as in (c), but for CTRL.

the downslope winds in the lee are more significant (Fig. 25a). Furthermore, winds in the wake zones off the Maui and Lanai coasts exhibit weak easterly wind anomalies. Our results confirm that the development of dual-rotating lee vortices is purely an inviscid process (Smolarkiewicz and Rotunno 1989).

The existence of the Maui vortex at night and the diagnostic analysis presented above suggest that solar heating and channeling effects are not essential for the occurrence of the Maui vortex. The land surface heating/cooling and latent heat release modify the airflow over land, including the lee vortices, and the wake circulations over the ocean offshore.

11. Summary and conclusions

In this study, we used the MM5/LSM initialized by the GFS to study island-scale airflow and circulations during July–August 2005, under summer trade wind conditions over Maui County. From our model results and model sensitivity tests, it is shown that the Maui vortex is the northern cyclonic vortex of the dual-counter-rotating vortices in the lee of Haleakala, which is a result of orographic blocking under a low-Fr (<1) flow regime and with mountain heights extending well above the trade wind inversion. The dual-rotating vortices extend up to the base of the trade wind inversion, with a dynamically

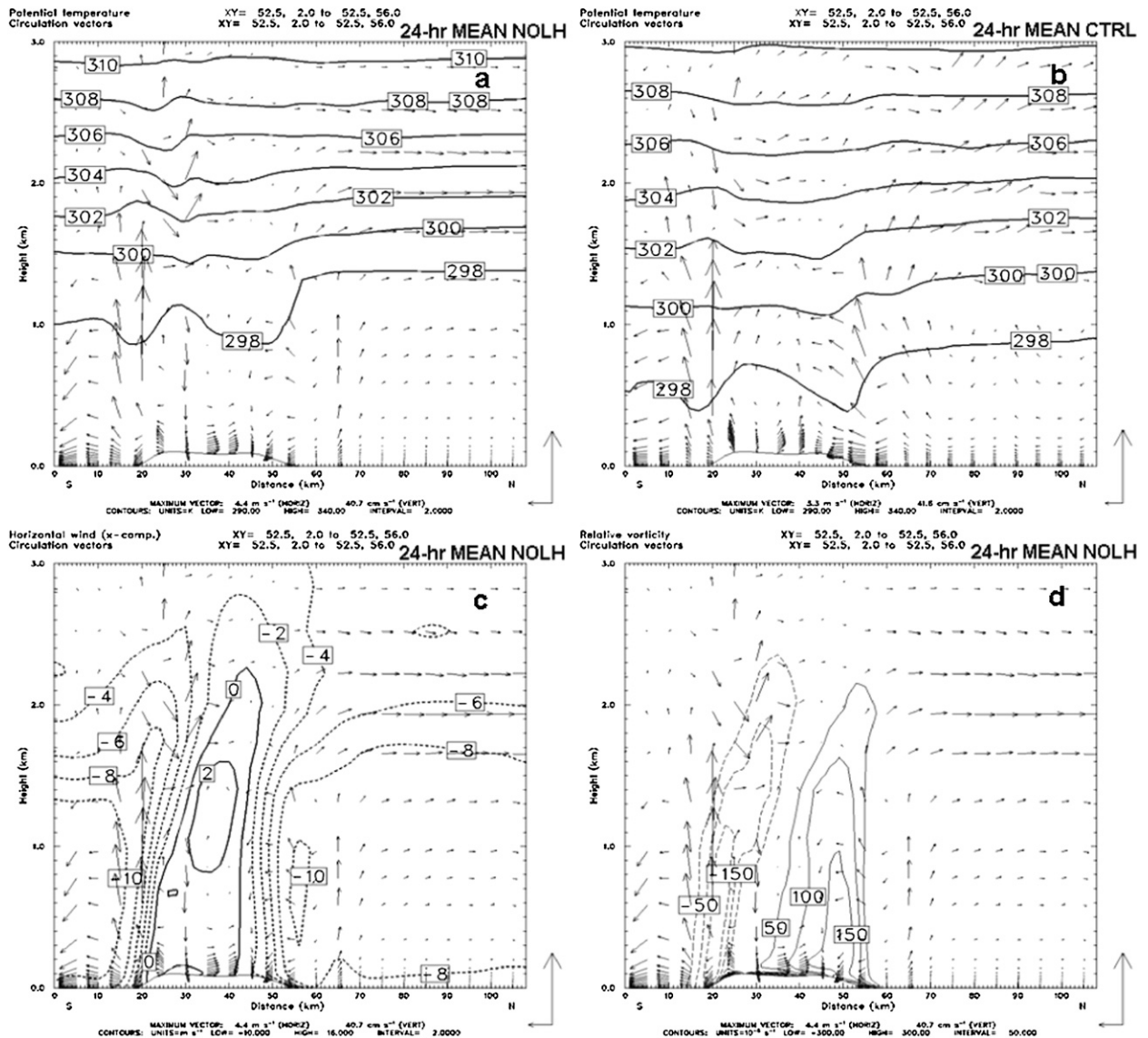


FIG. 24. The 24-h mean north–south vertical cross section (Fig. 6a) of (a) potential temperature (every 2 K) for the NOLH run. (b) As in (a), but for CTRL, (c) u -wind component (every 2 m s^{-1}), and (d) relative vorticity (every $40 \times 10^{-5} \text{ s}^{-1}$) for the NOLH run.

induced westerly reversed flow ($>2 \text{ m s}^{-1}$) along the axis and are modified by the land surface process during the diurnal heating cycle. The intensity of the lee vortices at the surface is also reduced slightly by surface friction. In low levels, the shape, and horizontal extent of the vortices are affected by flow deflection at the foothills of the West Maui Mountains and the shape of Haleakala.

In low levels, the Maui vortex is more pronounced than the southern anticyclonic vortex, which sometimes does not exhibit a closed circulation. At the surface, the Maui vortex has a relatively narrow ($\sim 10 \text{ km}$) east–west extent, but is elongated in the north–south direction because of the flow deflection by the West Maui Mountains.

For the flow past the West Maui Mountains, the layer averaged U/N (300–1700 m) is about 1200 m, which is smaller than h ($\sim 1770 \text{ m}$). Thus, the low-level flow is deflected on the windward side, especially at night. The northern coastline of Haleakala exhibits a convex shape associated with a ridge axis, whereas the southern coast has a more or less east–west orientation. The southern anticyclonic circulation is also affected by the island of Kahoolawe off the southwestern coast. Above the trade wind inversion, the flow past Haleakala is characterized by $Fr < 1$, with a weak hydraulic jump in the lee. The descending air above the trade wind inversion could pass the inversion boundary and reach the lower leeside slope.

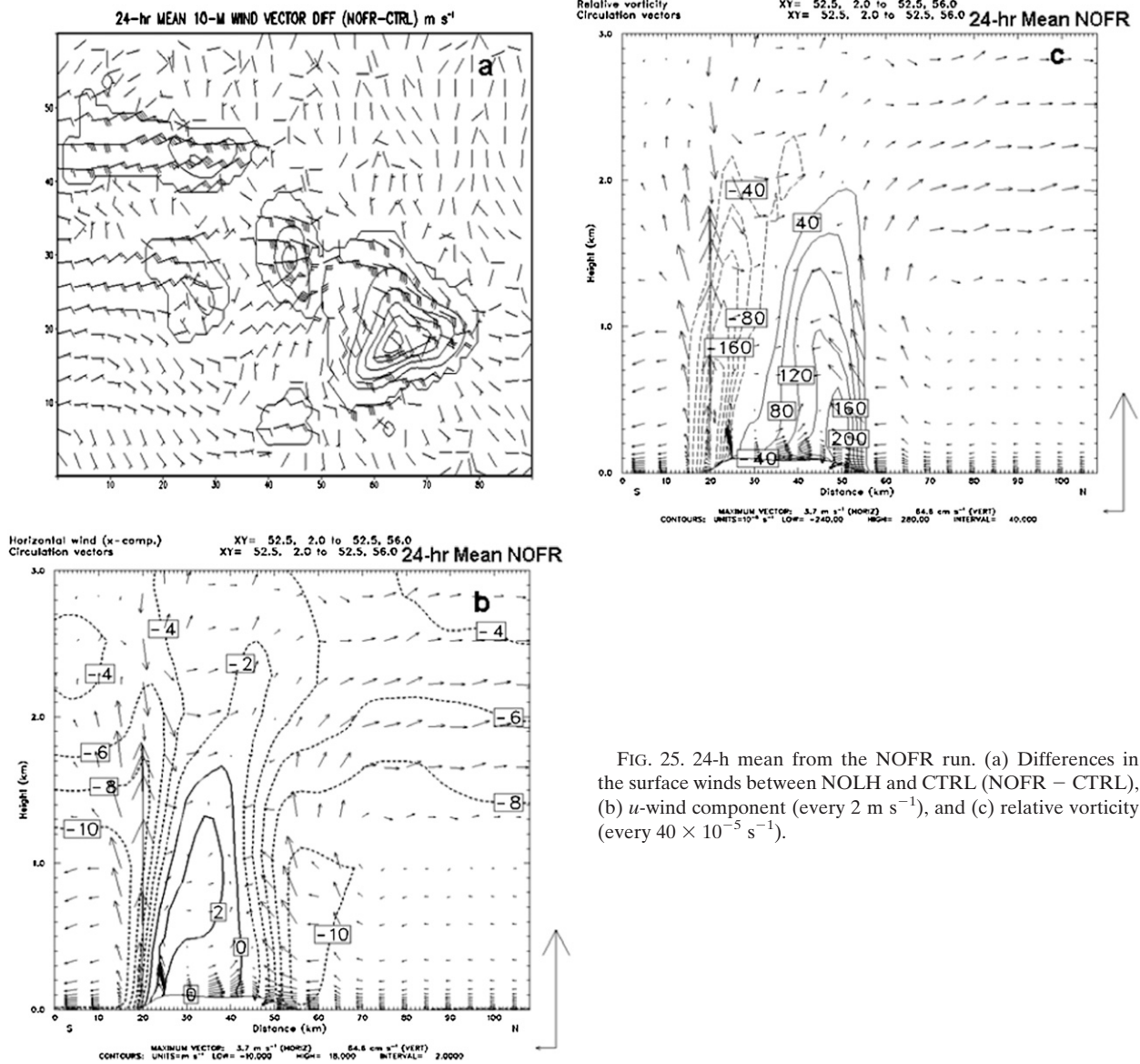


FIG. 25. 24-h mean from the NOFR run. (a) Differences in the surface winds between NOLH and CTRL (NOFR - CTRL), (b) *u*-wind component (every 2 m s⁻¹), and (c) relative vorticity (every 40 × 10⁻⁵ s⁻¹).

The wave breaking aloft is more significant at night than during the day.

In contrast to the lee vortices off the leeward coast of the island of Hawaii, the Maui vortex is mainly over land and is significantly modified by the diurnal heating cycle. At night, the westerly return flow at the surface in the lee of Haleakala is replaced by katabatic flow, with weak sinking motion. The surface flow over the Central Valley exhibits a weak closed circulation between strong northerly winds deflected by the West Maui Mountains and weak southeasterly katabatic winds from the leeward slopes of Haleakala. In the lee of the West Maui Mountains, dual-counter-rotating vortices are present below the 1-km level, with a hydraulic jump aloft. In the afternoon, the downslope winds and the hydraulic jump in the lee

of West Maui are weak, with combined westerly return/sea-breeze flow along the leeward coast.

At 1400 HST, anabatic/upslope winds develop on the leeward slopes of Haleakala. The Maui vortex is simulated between the anabatic/westerly reversed (>2 m s⁻¹) flow to the lee of Haleakala and strong easterly flow off the northern coast of the Central Valley. A southern anticyclonic circulation is also evident. With relatively weak orographic blocking by the West Maui Mountains, the low-level westerly reversed flow between the counter-rotating vortices in the lee of Haleakala extends offshore off the southwestern leeward coast. Above the surface, the westerly reversed flow in the lee is weaker, with a smaller east-west horizontal extent than at night in response to the development of daytime thermally induced upslope

flow on the leeside slopes. Off the leeside coasts of Maui and Lanai, low-level westerly flow in the wake zones, driven mainly by daytime heating over land, extends more than 40 km downstream.

The lee side of Haleakala is relatively dry with little precipitation. With relatively calm winds, clear skies, dry soils, and semiarid ground cover, the morning transition to the lee of Haleakala is completed within 2 h after sunrise. Above the trade wind inversion, the downslope flow to the lee of Haleakala and the hydraulic jump aloft also weaken after sunrise. The evening transition on the leeside slopes and Central Valley due to nocturnal cooling is a slow process. The onset of the easterly katabatic winds starts on the leeside slopes of Haleakala and progresses slowly downward over the Central Valley until around midnight. During the transition, the westerly return flow above the surface strengthens and extends westward.

The location, horizontal and vertical extent, and strength of the Maui vortex are also affected by the trade wind strength and latent heat release. The flow deflection by the northern ridge axis of Haleakala and the West Maui Mountains is more significant for weak trades than strong trades. As a result, the center of the Maui vortex at the surface is northward and closer to the foothills when trades are weaker. The westerly return flow to the lee of Haleakala is stronger (3 versus 1 m s^{-1}), for strong trades than for weak trades with stronger counter-rotating vortices extending above the trade wind inversion. Without latent heat release (NOLH), the orographic blocking over the West Maui Mountains and for the airflow below and above trade wind inversion is more significant. The latent heat release affects the location and intensity of the lee vortices. Furthermore, with a more pronounced trade wind inversion than in the control run, the lee vortices are also present above the trade wind inversion base in the NOLH run.

Acknowledgments. This work was funded by the NOAA Educational Partnership Program (EPP) Graduate Scientists Program (GSP), the National Weather Service Pacific Region, the USDA Forest Service under Agreement 05-JV-11272165-015, and COMET/UCAR under Grant S0975789. We thank Hiep Van Nguyen and David Hitzl for their assistance.

REFERENCES

- Austin, G. R., R. M. Rauber, H. T. Ochs III, and L. J. Miller, 1996: Trade wind clouds and Hawaiian rainbands. *Mon. Wea. Rev.*, **124**, 2126–2151.
- Carbone, R. E., W. A. Cooper, and W. C. Lee, 1995: Forcing of flow reversal along the windward slopes of Hawaii. *Mon. Wea. Rev.*, **123**, 3466–3480.
- Chen, F., and R. Avissar, 1994a: The impact of land-surface wetness heterogeneity on mesoscale heat fluxes. *J. Appl. Meteor.*, **33**, 1323–1340.
- , and —, 1994b: Impact of land-surface moisture variability on local shallow convective cumulus and precipitation in large-scale models. *J. Appl. Meteor.*, **33**, 1382–1401.
- , and J. Dudhia, 2001a: Coupling an advanced land surface–hydrology model with the Penn State–NCAR MM5 modeling system. Part I: Model implementation and sensitivity. *Mon. Wea. Rev.*, **129**, 569–585.
- , and —, 2001b: Coupling an advanced land surface–hydrology model with the Penn State–NCAR MM5 modeling system. Part II: Preliminary model validation. *Mon. Wea. Rev.*, **129**, 587–604.
- Chen, Y.-L., and A. J. Nash, 1994: Diurnal variation of surface airflow and rainfall frequencies on the island of Hawaii. *Mon. Wea. Rev.*, **122**, 34–56.
- , and J.-J. Wang, 1994: Diurnal variations of surface thermodynamic fields on the island of Hawaii. *Mon. Wea. Rev.*, **122**, 2125–2138.
- , and —, 1995: The effects of precipitation on the surface temperature and airflow over the island of Hawaii. *Mon. Wea. Rev.*, **123**, 681–694.
- , and J. Feng, 2001: Numerical simulations of airflow and cloud distributions over the windward side of the island of Hawaii. Part I: The effects of trade wind inversion. *Mon. Wea. Rev.*, **129**, 1117–1134.
- Colle, B. A., 2004: Sensitivity of orographic precipitation to changing ambient conditions and terrain geometries: An idealized modeling perspective. *J. Atmos. Sci.*, **61**, 588–606.
- Daniels, P. A., and T. A. Schroeder, 1978: Air flow in the Central Valley of Maui, Hawaii. *J. Appl. Meteor.*, **17**, 812–818.
- Dudhia, J., 1989: Numerical study of convection observed during the winter monsoon experiment using a mesoscale two-dimensional model. *J. Atmos. Sci.*, **46**, 3077–3107.
- , 1993: A nonhydrostatic version of the Penn State–NCAR Mesoscale Model: Validation tests and simulation of an Atlantic cyclone and cold front. *Mon. Wea. Rev.*, **121**, 1493–1513.
- Epifanio, C. C., and R. Rotunno, 2005: The dynamics of orographic wake formation in flows with upstream blocking. *J. Atmos. Sci.*, **62**, 3127–3150.
- Esteban, M. A., and Y.-L. Chen, 2008: The impact of trade wind strength on precipitation over the windward side of the Island of Hawaii. *Mon. Wea. Rev.*, **136**, 913–928.
- Feng, J., and Y.-L. Chen, 1998: The evolution of katabatic flow on the island of Hawaii during 10 August 1990. *Mon. Wea. Rev.*, **126**, 2185–2199.
- , and —, 2001: Numerical simulations of airflow and cloud distributions over the windward side of Hawaii. Part II: Nocturnal flow regime. *Mon. Wea. Rev.*, **129**, 1135–1147.
- Frye, J., and Y.-L. Chen, 2001: Evolution of downslope flow under strong opposing trade winds and frequent trade wind rain-showers over the island of Hawaii. *Mon. Wea. Rev.*, **129**, 956–977.
- Garrett, A. J., 1980: Orographic cloud over the eastern slopes of Mauna Loa Volcano, Hawaii, related to insolation and wind. *Mon. Wea. Rev.*, **108**, 931–941.
- Giambelluca, T. W., M. A. Nullet, and T. A. Schroeder, 1986: Rainfall atlas of Hawaii. Rep. R76, Department of Land and Natural Resources, Honolulu, HI, 267 pp.
- Grell, G. A., 1993: Prognostic evaluation of assumptions used by cumulus parameterization. *Mon. Wea. Rev.*, **121**, 764–787.
- Hong, S.-Y., and H. L. Pan, 1996: Nonlocal boundary layer vertical diffusion in a medium-range forecast model. *Mon. Wea. Rev.*, **124**, 2322–2339.

- Hsie, E.-Y., R. A. Anthes, and D. Keyser, 1984: Numerical simulation of frontogenesis in a moist atmosphere. *J. Atmos. Sci.*, **41**, 2581–2594.
- Juang, H. H.-M., 2000: The NCEP mesoscale spectral model: A revised version of the nonhydrostatic regional spectral model. *Mon. Wea. Rev.*, **128**, 2329–2362.
- Kodama, K. R., and S. Businger, 1998: Weather and forecasting challenges in the Pacific region of the National Weather Service. *Wea. Forecasting*, **13**, 523–544.
- Lavoie, R. L., 1967: Air motions over the windward coast of the island of Hawaii. *Tellus*, **19**, 354–358.
- Leopold, L. B., 1949: The interaction of trade wind and sea breeze, Hawaii. *J. Meteor.*, **6**, 312–320.
- Li, J., and Y.-L. Chen, 1999: A case study of nocturnal rainshowers over the windward coastal region of the island of Hawaii. *Mon. Wea. Rev.*, **127**, 2674–2692.
- Miglietta, M. M., and A. Buzzi, 2001: A numerical study of moist stratified flow over isolated topography. *Tellus*, **53A**, 481–499.
- Nguyen, H. V., Y.-L. Chen, and F. M. Fujioka, 2010: Numerical simulations of island effects on airflow and weather during the summer over the island of Oahu. *Mon. Wea. Rev.*, **138**, 2253–2280.
- Nickerson, E. C., and M. A. Dias, 1981: On the existence of atmospheric vortices downwind of Hawaii during the HAMEC project. *J. Appl. Meteor.*, **20**, 868–873.
- Reisner, J. M., and P. K. Smolarkiewicz, 1994: Thermally forced low Froude number flow past three-dimensional obstacles. *J. Atmos. Sci.*, **51**, 117–133.
- Rotunno, R., V. Grubisic, and P. K. Smolarkiewicz, 1999: Vorticity and potential vorticity in mountain wakes. *J. Atmos. Sci.*, **56**, 2796–2810.
- Schär, C., and R. B. Smith, 1993: Shallow-water flow past isolated topography. Part I: Vorticity production and wake formation. *J. Atmos. Sci.*, **50**, 1373–1400.
- , and D. R. Durran, 1997: Vortex formation and vortex shedding in continuously stratified flows past isolated topography. *J. Atmos. Sci.*, **54**, 534–554.
- Schroeder, T. A., 1993: Climate controls. *Prevailing Trade Winds: Climate and Weather in Hawaii*, M. Sanderson, Ed., University of Hawaii Press, 12–36.
- Smith, R. B., and V. Grubišić, 1993: Aerial observation of Hawaii's wake. *J. Atmos. Sci.*, **50**, 3728–3750.
- Smolarkiewicz, P. K., and R. Rotunno, 1989: Low Froude number flow past three-dimensional obstacles. Part I: Baroclinically generated lee vortices. *J. Atmos. Sci.*, **46**, 1154–1164.
- , R. M. Rasmussen, and T. L. Clark, 1988: On the dynamics of Hawaiian cloud bands: Island forcing. *J. Atmos. Sci.*, **45**, 1872–1905.
- Ueyoshi, K., J. O. Roads, F. Fujioka, and D. E. Stevens, 1996: Numerical simulation of the Maui vortex in the trade winds. *J. Meteor. Soc. Japan*, **74**, 723–744.
- Yang, Y., and Y.-L. Chen, 2003: Circulations and rainfall on the lee side of the island of Hawaii during HaRP. *Mon. Wea. Rev.*, **131**, 2525–2542.
- , and —, 2008: Effect of terrain heights and sizes on island-scale circulations and rainfall. *Mon. Wea. Rev.*, **136**, 120–146.
- , —, and F. Fujioka, 2005: Numerical simulations of the island-induced circulations over the island of Hawaii during HaRP. *Mon. Wea. Rev.*, **133**, 3693–3713.
- Zhang, Y., Y.-L. Chen, S.-Y. Hong, K. Kodama, and H.-M. H. Juang, 2005a: Validation of the coupled NCEP Mesoscale Spectral Model and an advanced Land Surface Model over the Hawaiian Islands. Part I: Summer trade wind conditions over Oahu and a heavy rainfall event. *Wea. Forecasting*, **20**, 847–872.
- , —, and K. Kodama, 2005b: Validation of the coupled NCEP Mesoscale Spectral Model and an advanced land surface model over the Hawaiian Islands. Part II: A high wind event. *Wea. Forecasting*, **20**, 873–895.